# 2018 25th Congress of International Federation for Heat Treatment and Surface Engineering

*11-14 September 2018 | Xi`an China*

# PROCEEDINGS

Organized by Chinese Heat Treatment Society（CHTS）

# 25th IFHTSE CONGRESS PROCEEDINGS

11-14 September 2018

Xi'an China


Chinese Heat Treatment Society

*Tel：+86（0）10 6292 0613 • Email：chts@chts.org.cn • Web:www.chts.org.cn*

*Add: 18 Xueqing Rd.,Beijing,China*

Failure analysis of leakage of valve tube in drain pipeline in nuclear power plant.....576
Failure analysis of leaking small-diameter buried 20 steel pipe.....576
Helicalspring fracture failure analysis of suspension for vehicle.....576
Peridynamic simulation of crack formation and propagation in pitting corrosion of carbon steel pipes.....577
Failure case analysis—failure analysis of casing head slip hanger.....577
Failure analysis of welded chain slings used for lifting purpose in oil and gas industry.....578
Investigation on impact absorbed energy index of drill pipe.....578
Failure analysis of sulfide stress corrosion cracking on P105 tubing coupling.....579
Experimental study on temperature effect of high performance casing material in deep well and ultra-deep well.....579
Fracture control of the 2nd west east gas pipeline.....580
Fracture failure analysis on ultra supercritical turbine bolts.....580
Research on the performance of hollow bolt yield ratio of 45 steel.....581
Failure analysis of a P110 grade non-API anti-sulfide corrosion tubing coupling used in ultra deep oil well.....581
A phase transformation to predict the high contact stress in bearing steel due to rolling contact fatigue.....582
Cracking failure analysis on L245NS steel grade elbow.....582
Fracture failure analysis of C110 casing in sour oil and gas field.....583
EIS studies of the resistance-reducing internal coating of in-service natural gas pipeline.....583

## Microstructure and Properties

Effect of Si and Cr on surface microstructure formed by lithium doped salt-bath nitrocarburizing in Fe-0.4wt%C.....584
Preparation of $Mo_5SiB_2$ powder by mechanical alloying and annealing.....585
The effect of twins and substructures evolution on dynamic recrystallization behaviors in Ni-30Fe austenitic alloy.....586
The high-temperature tensile behaviors of vanadium-containing 25Cr-20Ni austenitic stainless steels.....588
Effect of {332} <113> twinning on Charpy impact behavior in metastable β-type Ti-15Mo alloy.....590
Fabrication, structure, and thermal stability of electroless Ni-Fe-P coating.....591
Surface characterization of a selectively dissolved Ni-Ni3Si eutectic alloy.....592
Preparation of molybdenum copper composite powder by wet chemical method and its sintering properties.....593
The effect of post-weld heat treatment on the carbide evolution of Hastelloy N alloy in heat affected zone.....594
Effect of annealing temperature on texture and magnetic properties of 6.5%Si ultra-thin strip.....594

Fatigue life enhancement mechanism of TB9 Hi-bolt.....595
Evaluation method of fatigue life based on damage mechanics.....595
Microstructure and mechanical property of Al/SiCp nanocomposite coating produced by cold spraying of ball-milled powder.....596
Phase transformation and irradiation effects of BN/BAS ceramic composites induced by charged argon ion beam.....596
Effect of tempering temperature on low carbon bainite steel plate.....597
Influence of ferrite content and tempering temperature on the mechanical properties of HSLA steel.....597
CCT curves and microstructure of a new type bainitic wear-resistant casting steel.....598
Effect of quenching temperature on the microstructure and corrosion behavior of X80 pipeline steel.....598
Microstructure and mechanical properties of uranium alloy impacted by steel projectile under different velocities.....599
Effect of annealing temperature on the microstructure and mechanical properties of the ferrtic rolling low carbon steel sheet.....599
The effect of precipitation on the property of high strength steel plates under different heat treatment techniques.....600
Investigations of the tensile properties and fracture characteristics of amorphous ribbons Fe81.50B1.40Si7.95Nb7.37Cu1.728 alloy.....600
Several methods of reducing the testing errors in rockwell hardness.....601
Evolution of microstructure and strain-induced precipitates in Nb-Ti extra heavy slab during hot-core heavy reduction rolling.....601
Microstructure and mechanical properties of in situ Mo/$Mo_2C$ composite.....602
Influence of Si/B ratio on microstructural evolution and properties of ultrafine-grained Mo-$Mo_3Si$-$Mo_5SiB_2$ alloys doped with $La_2O_3$.....603
Improvement of fracture toughness in Mo-Si-B alloy with a microstructure of bimodal α-Mo phase.....604
Effect of austempering process on the microstructure and properties of D2 cold work die steel.....605
Effect of heat treatment parameters on microstructure and mechanical properties of a modified AISI 4140 steel.....606
Production and characterization of vermicular graphite steel with 2% carbon.....607
Obtaining the TTT diagrams for graphitic steels alloyed with niobium.....608
Microstructural study of ODS alloy with hafnium and yttrium addition.....609
Selection of heat treatment process parameters of H13 hot die steel based on orthogonal test.....610
Characterization and optical properties of SnS nano-plate prepared by solvothermal method.....611
Effects of niobium addition and aging treatment on the microstructural changes and mechanical properties of the Fe-30Mn-7Al-1.1C alloy.....612
Microstructure and mechanical properties of W-Si composites by spark plasma sintering.....613

Effect of thermal exposure on microstructure and mechanical properties of an Al-Zn-Mg-Cu alloy....614
Study on static recrystallization of austenite during hot deformation of heavy rail steel....614
Formation of high strength and high plasticity nano/ultrafine structure by martensite reversion in 18Cr-8Ni austenitic stainless steel....615
Aging analysis on low carbon cold rolled steel sheet during rapid heating treatment....615
Research on corrosion of 0.3C-14Cr-0.5Ni powder/2Cr13 laser heterogeneous coating....616
Effect of solution temperature on microstructure and mechanical properties of Ti-5Al-5Mo-5V-3Cr-1Zr titanium alloy....616
Comparison of microalloying effects with Ca and Ce on corrosion properties of extruded Mg-3Al-1Zn alloy....617
Nanoindentation investigation on the 18Cr-8Ni austenitic stainless steels with grain size from nano/ultrafine-grain to coarse grain....617
Effect of heat treatment on mechanical property and microstructure of a low nickel superalloy for exhaust engine valves....618
The effect of VC precipitation on the properties of medium carbon high alloyed steel....618
Effect of volume fraction of retained austenite on the scratch and abrasion resistance of AISI 321 metastable austenitic stainless steel....619
Study on aluminum alloy micro-arc oxidation coating thickening reaction mechanism....619
Insight into the microstructure of the surface oxidation layer of nitrogen-rich uranium nitride....620
A New TiC reinforced low alloy abrasion resistant steel....620
Processing and properties of nanostructured $TiB_2$-NiCrCoAlY composite powders via spray drying and plasma spheroidization....621
Different effect of annealing on the microstructure of supersaturated Cu-Cr alloy film and bulk....621
Characterization and wear behaviors of SUJ 2 steel in different microstructure....622
Effects of process parameters on content of fluorine and zirconium in oxidation film formed on magnesium alloys....622
Current status of understanding of alloy element effects on α/β transformations in steel....623
Research progress on controlled solidification and its applications....623
Aging behavior of 6061Al matrix composite reinforced with high content SiC nanowires....624
Corrosion resistance of HiPIMS-TiN coatings sealed by ALD-Layers with and without $N^+$ pre-ion-implantation....625

# Effect of Si and Cr on surface microstructure formed by lithium doped salt-bath nitrocarburizing in Fe-0.4wt%C

Haruna Ishizuka[1], Youichi Watanabe[1], Masao Takeyama[2]
(1. Parker Netsushori Kogyo Co., Ltd.; 2. Tokyo Institute of Technology)
h.ishizuka@pnk.co.jp

**Abstract:** Mold technology in Japan is the best in the world, and it is important for automotive parts manufacturing industries to be more competitive and productive. Die-casting using mold is well known to be one of the manufacturing processes for automotive engine blocks. Surface hardening treatments such as gas-nitriding or -nitrocarburizing have been applied to die-casting molds in the aim of increasing lifetime. These treatments are usually employed at temperatures below austenitizing temperature by diffusing nitrogen (or nitrogen and carbon) into steels from the surfaces under nitrocarburizing environments. Since the casting conditions are becoming more severe, the demands for new surface modification technologies are becoming expanded.

Recently a novel salt-bath nitrocarburizing process by adding lithium ions to the molten salt was developed, and it has already been successfully applied to mass production for some automobile parts. The novel process can improve erosion and seizure resistance of molds because of the formation of thicker and denser oxide layer in concurrence with a nitrided layer, in comparison with those formed by conventional post-oxidized treatment. Therefore, there are expectations to apply this treatment to die mold. However, the microstructure and its formation process of the surface layer in steels containing some alloying elements during the nitrocarburizing process have not yet been fully understood. In this study, thus, the effect of alloying elements on the formation of surface microstructure during the novel salt-bath nitrocarburizing has been examined by using model steels. Focus is placed on silicon (Si) and chromium (Cr), since these elements are common in hot-die steels.

Alloys used in this study are Fe-0.4wt%C and ones containing Si and Cr by 2wt% independently. These alloys were prepared by arc melting into 30 g button ingot under Ar atmosphere. The ingots were annealed at 1123 K for 1 h, followed by air cooling and double tempered at 873 K, similar to the heat treatments employed to hot die steels. Salt-bath nitrocarburizing was carried out at 823 K for 0.1 h up to 10 h. Microstructure of the cross sectional surface regions of the specimens were examined using optical microscope and FE-SEM. Elemental mapping as well as phase identification of the surface regions were done by EDS and XRD, respectively.

In the binary alloy, a continuous thin surface oxide layer of $LiFeO_2$ forms first at the beginning of the process, followed by formation of nitrogen compound layer (NCL). As the process proceeds, the oxide layer becomes thick to about 10 μm in thickness, and internal oxidation takes place along the grain boundaries in the NCL. Cr addition makes the formation of oxide layer sluggish, and also suppresses the internal oxidation, but it has little effect on the growth kinetics of the NCL. In contract, addition of Si enhances the oxide layer but suppresses the internal oxidation in the NCL formed underneath the oxide layer. Although, little effect is observed for the formation of NCL, much further penetration of nitrogen is locally observed, indicating that diffusion of nitrogen is somehow enhanced. The change in the microstructure by the alloying is closely related to the morphology change of the outmost oxide layer.

**Keywords:** surface microstructure, salt bath nitrocarburizing

# Preparation of $Mo_5SiB_2$ powder by mechanical alloying and annealing

Yao Zhang, Guojun Zhang
(School of Materials science and Engineering, Xi'an University of Technology)
zhangguojun@xaut.edu.cn

**Abstract:** With the improvement of mechanical design, the performance of internal combustion engine has been greatly improved. While higher performance, higher requirements for high temperature structural materials in internal combustion engine have been put forward. Therefore, the study of new high-temperature structural materials has more practical significance. The $Mo_5SiB_2$ (T2) phase has a high melting point (2160 ℃) and a relatively low density (8.86 g/cm$^3$), belonging to intermetallic phases, with high strength, hardness and poor plastic deformation ability. In 1273 K, T2 can exhibit superior oxidation resistance, in contact with air layer, Si and B in the T2 phase are captured by oxygen to form a glass phase, and due to the presence of B glass phase with good fluidity can be covered on the surface, thereby preventing oxygen into the matrix.

In order to develop a method for the preparation of Mo5SiB2 alloy powder, the phase composition and micromorphology of $Mo_5SiB_2$ alloy powder was investigated after mechanical alloying and annealing. The $Mo_5SiB_2$ powders with slight change in composition(Mo-12Si-26B at%, Mo-12.6Si-25.2B at%, Mo-12.7Si-25.4B at%, Mo-13Si-26B at%) were manufactured via a mechanical alloying process followed by annealing and mechanical crushing. Mo, Si and B powders were milled in planetary ball milling(Retsch PM400, WC balls and WC vial) with 250 rpm speed and a powder-to-ball weight ratio 1:15 in planetary ball milling under Ar atmosphere. The mixed alloy powders were annealed for 2 hours at 1450 ℃ in vacuum. The phase composition was determined by XRD, and the morphology of the powder was observed by SEM and the particle size was evaluated. The XRD test results show that all the alloy powders contain T2 phase and it can be preliminarily determined that the powder with the T2 phase as the main phase can be prepared by mechanical alloying + annealing. Due to the mechanical alloying process, a small amount of $W_2C$ particles were distributed in the powder. Because the ratio of Si and B does not reach 1:2, there is a weak Mo diffraction peak in Mo-12Si-26B at% powder. No other secondary phases were found in other powders with Si and B ratios of 1:2. The results of scanning electron microscopy showed that the alloy particles after annealing had four prismatic morphology, and the particle size was about 1-10 μm.

The experimental results show that the T2 phase powder with certain purity can be prepared by mechanical alloying and annealing. When the ratio of Si and B is not maintained at 1:2, the second phase will be generated. The obtained particle morphology is prismatic. Therefore, T2 phase powder can be added to other alloy matrix as an augmented particle, thereby improving mechanical properties and high temperature oxidation resistance.

**Keywords:** $Mo_5SiB_2$, mechanical alloying, superalloy

# The effect of twins and substructures evolution on dynamic recrystallization behaviors in Ni-30Fe austenitic alloy

Wenxiong Chen[1], Chengwu Zheng [2], Dianzhong Li[2]
(1. Shenyang National Lab. for Materials Science, Institute of Metal Research, CAS;
2. School of Materials Science and Engineering, University of Science and Technology of China)
wxchen14s@imr.ac.cn

**Abstract:** Dynamic recrystallization (DRX) is an important restoration process that occurs during hot working of many metallic materials, which can refine the microstructures by introducing new grains with high angle grain boundaries (HAGBs). It provides an alternative approach to optimize the grain structures by controlling hot working under appropriate conditions so as to improve the mechanical properties of final products. This requires a detailed understanding about fundamentals of the DRX behavior itself. In this purpose, the microstructural behavior of dynamic recrystallization of austenite is investigated from the aspect of evolution of twins and substructures in a Ni-30Fe austenitic model alloy. Here, a Gleeble3500 thermo-mechanical simulator was used to execute hot compression tests to various strains under a stain rate of $0.01s^{-1}$ at 1000 ℃ following with rapid water quenching subsequently. Microstructural characteristics of twins and sub-boundaries were then analyzed by EBSD in conjunction with TEM.

The microstructural analysis indicates that strain-induced migration of the pre-existing boundaries and triple junctions accompanied by the formation of geometrically necessary boundaries (GNBs) and twinning is the prominent mechanism for DRX nucleation. And the twinning mechanism shows much easier than that by the formation of GNBs. Actually, a large proportion of twin boundaries (i.e. about 50 pct length fraction of pre-existing HAGBs) exist in the Ni-30Fe sample before the hot deformation. And this fraction is found varied with the hot deformation progressing through competition between the deviation of the pre-existing twin boundaries caused by the continuing deformation and formation of the new twin boundaries accompanied with the grain boundaries migrations. The deviation of the pre-existing twin boundaries is ascribed to the interaction of dislocations with the twin boundaries. The TEM observation confirms that dislocations could glide through the twin boundaries, which either results in twin steps or leads to gradually conversion of the twin boundaries towards general boundaries due to dislocation trapping at the twin boundaries as seen in Fig.1. The twin steps could be acted as favorable sites for DRX nucleation during further deformations. The mechanism of new twinning by growth accidents associated with grain boundaries migration can lead to DRX nucleation occurred at a relatively low strain because of the deformation inhomogeneities around triple junctions and pre-existing boundaries. And abundance of twins generated during the stage of the grain growth owing to large scales of grain boundaries migration, which might cut down grain boundary energies of recrystallized grain and facilitate further growth.

The TEM results further validate that dislocations are readily to arrange in the sub boundaries. A few of sub-boundaries are found translated into GNBs. Misorientations between them are increased by absorbing free dislocations in further deformation, as seen in Fig.2. The GNBs formed at the triple junctions and the bulged pre-existing boundaries are found easily transform into new DRX nuclei. And the intragranular GNBs prefer to evolve and transform into HAGBs gradually, which might promote DRX process by the CDRX mechanism.

In summary, both twins' evolution (i.e. new twinning and deviation of pre-existing twin boundaries) and sub-boundaries development can significantly influence the nucleation and growth of the DRX process in

austenite during hot deformation. Moreover, for the purpose of optimize microstructure, further work is required to study the effect of deformation paraments on the evolution of twins and substructures.

**Keywords:** dynamic recrystallization, twins, sub-boundaries, austenite

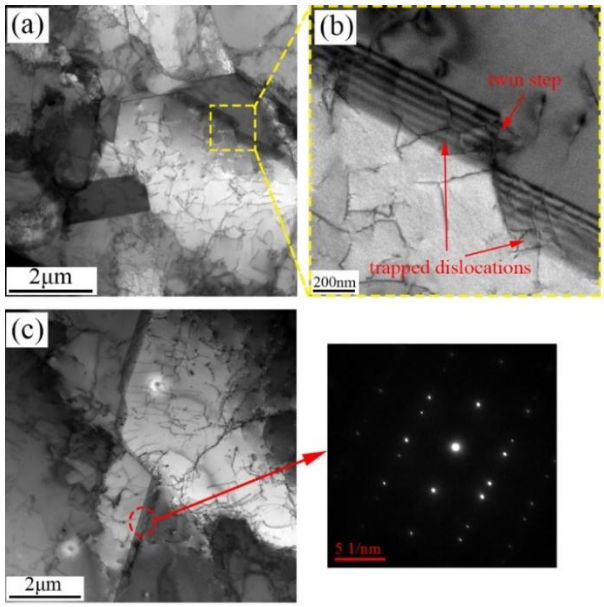


Fig.1 TEM images of interaction of twin boundaries and dislocations at strain of 0.2

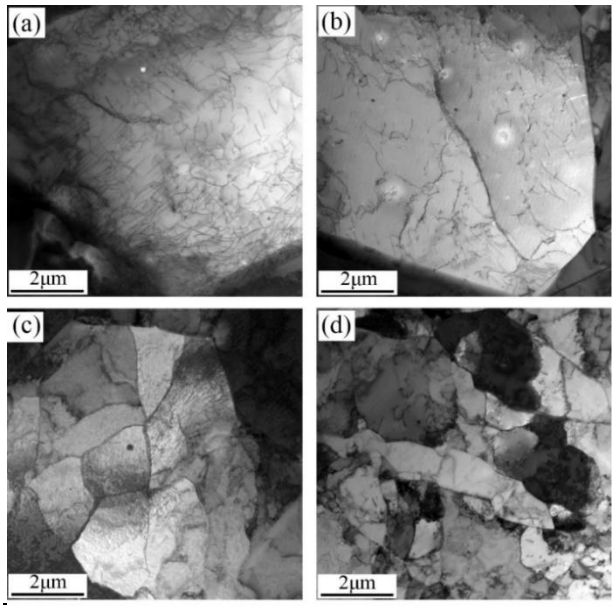


Fig.2 TEM images of dislocations arranged in sub-boundaries and translated as GNBs at different strains: (a)0.05; (b)0.1; (c)0.2; (d)0.5

# The high-temperature tensile behaviors of vanadium-containing 25Cr-20Ni austenitic stainless steels

Guodong Hu, Pei Wang, Shenghua Zhang, Dianzhong Li, Yiyi Li
(Shenyang National Laboratory for Materials Science, Institute of Metal Research)
gdhu13s@imr.ac.cn, pwang@imr.ac.cn

**Abstract:** To investigate the tensile behaviors of 25Cr-20Ni austenitic stainless steel at different temperatures, the high-temperature tensile tests of two 25Cr-20Ni austenitic stainless steels with different V concentration (0wt% V and 0.3wt% V, respectively) have been conducted at temperature between 200 ℃ and 900 ℃.

Two different austenitic stainless steels, Fe-24Cr-19Ni-1.7Mn-0.9Si-0.06C-0.06N and Fe24Cr-19Ni-1.5Mn-0.6Si-0.06C-0.06N-0.3V, were prepared by vacuum induction melting in laboratory. The ingots were forged first and solute treated at 1100 ℃ for 1 h followed by water quenching. Rod tensile specimens with diameter of 5 mm and gauge length of 25 mm were prepared according to GB/T 4336-2006 for high temperature tension. Tensile tests were performed on an MTS E45. 105 machine between 200 ℃ and 900 ℃ at interval of 100 ℃ in air with strain rate of $10^{-4}$ $s^{-1}$ before yielding and $1.3\times10^{-3}$ $s^{-1}$ after yielding. After tensile tests, the tensile properties over the test temperature range have been analyzed. The microstructure of the sample including the morphology of precipitates was observed by SEM. The grain boundary and grain orientation color maps obtained by EBSD were used to reveal the recrystallization. The dislocation configuration and precipitates evolution before and after tensile tests at different temperatures were observed using TEM to clarify the deformation mechanisms at various test temperatures.

Results show that the ultimate tensile strength of both steels is strong temperature dependent, which decreases slowly first at 200-300 ℃, keeps platform then at 300-500 ℃ and decreases rapidly afterwards from 600 ℃ to 900 ℃. The tensile strength variation with temperature is caused by the decreasing strain hardening ability, dynamic strain aging and dynamic recovery together with dynamic recrystallization at different temperatures.

Although the tensile strength of both steels decreases rapidly at 700 ℃ due to the dynamic recovery, the elongation of both steels does not increase accordingly. This is because the deteriorated effects of $M_{23}C_6$ precipitates at grain boundary. $M_{23}C_6$ carbides are formed at grain boundary during tensile test at 700 ℃ in both 0 V and 0.3 V steel, which promote crack formation at grain boundary and lead to a lower elongation. As the test temperature increases to 800 ℃, the elongation of both steels increases markedly due to the dynamic recovery and dynamic recrystallization.

Additionally, the V-containing 0.3 V steel has a relatively lower elongation at 800 ℃ and 900 ℃ compared to that of 0 V steel. This is because the solute V in 0.3 V steel retards the recrystallization due to the solute drag effects, while recrystallization can depress the crack initiation and propagation during tensile test. EBSD results show that fine recrystallized grains are formed at original grain boundaries after tested at 800 ℃ and the number of fine grains in 0 V steel is significantly larger than that in 0.3 V steel. The precipitate observation indicates that the addition of V induces little difference in the amount and size of MX precipitates after tensile test at 700-900 ℃. According to the thermodynamic calculation, the concentration of V in the matrix of 0.3 V steel at 800-900 ℃ is about 0.2wt%. It is reasonably inferred that the solute V induces a lower recrystallization degree in 0.3 V steel, further leading to a lower elongation of 0.3 V steel than 0 V steel.

**Keywords:** microstructure, carbide, mechanical property, toughness, AISI 4140, heat treatment parameters

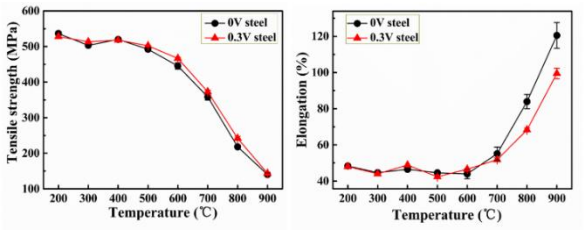


Fig.1 The variation in (a) UTS and (b) elongation of investigated steels with test temperature

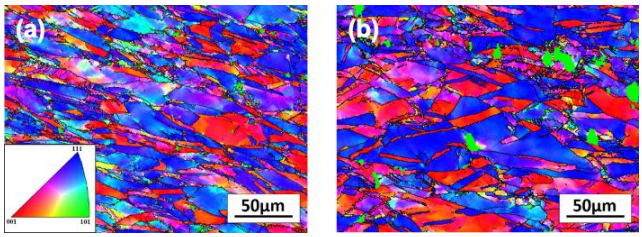


Fig.2 The grain orientation color maps of the researched steels subjected to tensile tests at 800 ℃ (a) 0 V steel (b) 0.3 V steel

Fig.3

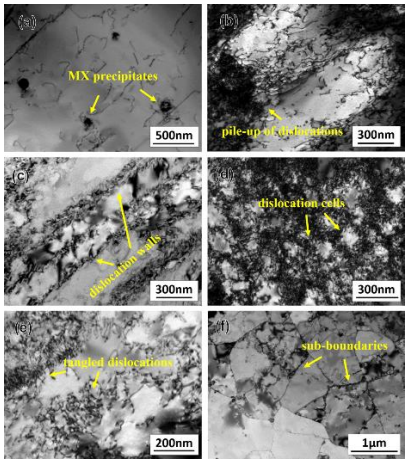


Fig.4

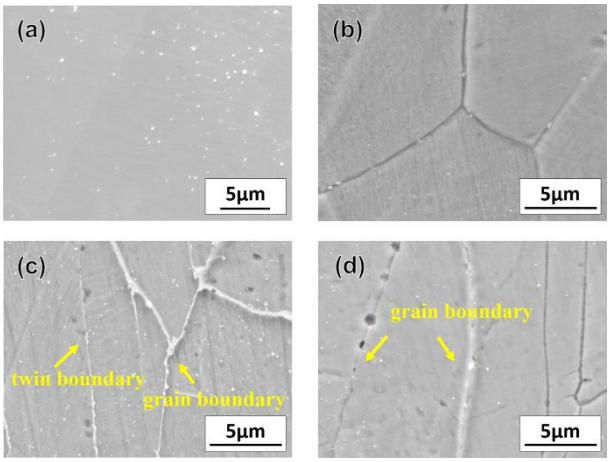


Fig.3 TEM micrographs of 0.3 V steel in (a) solution condition and after tensile test at: (b) 200 ℃, (c) 300 ℃, (d) 500 ℃, (e) 700 ℃, (f) 900 ℃

Fig.4 SEM micrograph of the samples after tested at different temperatures (longitudinal section): (a) 0.3 V steel tested at 200 ℃ (b) 0.3 V steel tested at 500 ℃ (c) 0.3 V steel tested at 700 ℃ (d) 0.3 V steel tested at 900 ℃

Fig.5

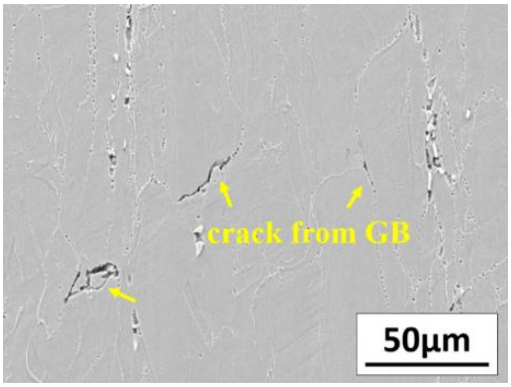


Fig.6

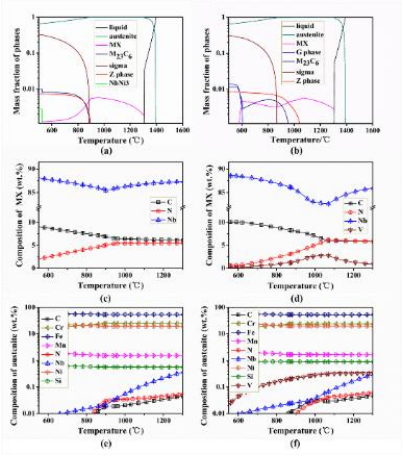

Fig.5 SEM micrograph of cracks formed at the GB with $M_{23}C_6$ carbides in 0.3 V steel at 700 ℃

Fig.6 Mass fraction of constitute phases in (a) 0 V steel and (b) 0.3 V steel; the composition of MX precipitates in (c) 0 V steel and (d) 0.3 V steel; and the composition of austenite matrix in (e) 0 V steel and (f) 0.3 V steel calculated by Thermo-Calc software

# Effect of {332} <113> twinning on Charpy impact behavior in metastable β-type Ti-15Mo alloy

Kai Yao[1], Xiaohua Min[1], Satoshi Emura[2], Koichi Tsuchiya[2]
(1. Dalian University of Technology; 2. National Institute for Materials Science)
minxiaohua@dlut.edu.cn

**Abstract:** Titanium and its alloys are widely used in fields of aerospace, biomedical application and energy industries due to their high specific strength, low elastic modulus and excellent corrosion resistance. Relatively low impact toughness, which is an important mechanical property for materials to be applied as structural parts for avoiding disastrous fracture[1], severely restricts their further industrial applications. Metastable β-type titanium alloys have been attracted extensive attention due to their good combination of strength and ductility via controlling deformation mode. For example, the Ti-15Mo alloy with {332}<113> twinning-induced plasticity (TWIP) effect exhibits a large uniform elongation through substantial work hardening behavior[2]. However, its impact toughness has not been comprehensively investigated. Thus, the purpose of present study is to investigate the Charpy impact behavior in a TWIP Ti-15Mo alloy, and to discuss the effect of mechanical twins on the crack initiation and its propagation behaviors.

A {332}<113> twinning-type Ti-15Mo alloy was prepared by cold crucible levitation melting as well as a dislocation slip-type Ti-15Mo-1Fe alloy as a comparison material. The ingots were subjected to homogeneous treatment, hot forging, multi-pass caliber rolling and solution treatment. The standard Charpy impact samples with V-type notch were machined and tested. Fracture morphologies were observed via field emission scanning electron microscopy (FE-SEM, JEM-7001F). Deformation microstructures on vertical section perpendicular to the notch were observed through optical microscopy (OM, VHX-600) and electron backscattered diffraction (EBSD) measurements, which were performed on FESEM (Zeiss-Σigma) equipped with an orientation imaging system.

Twinning-type Ti-15Mo alloy exhibited excellent Charpy impact energy (200 J), which was four times higher than that for slip-type Ti-15Mo-1Fe (50 J). Both alloys exhibited the ductile dimple fracture under impact loading. In Ti-15Mo alloy, the elongated and small dimples as well as serpentine glide morphology were observed on impact fracture surface, while the shallow and big dimples were characterized in Ti-15Mo-1Fe alloy. Abundant {332}<113> twins were formed in Ti-15Mo alloy, resulting in the extensive plastic deformation, while the twin formation was limited in Ti-15Mo-1Fe alloy. The existence of dense and fine twins effectively released the stress concentration due to the dynamic microstructural refinement effect, therefore delaying the initiation of micro-crack. The micro-cracks were significantly dispersed via propagating along the twin boundaries, which resulted in the substantial consumption of fracture energies to further enhance the impact toughness. Consequently, {332}<113> twinning provided an efficient approach for obtaining titanium alloys with optimal match of high strength and toughness.

**Keywords:** titanium alloy, {332}<113> twinning, impact toughness, crack initiation and propagation

# Fabrication, structure, and thermal stability of electroless Ni-Fe-P coating

Juan Peng[1], Xueming Du[1], Zhiwen Chen[2], Han Zhang[1], Li Liu[1]
(1. School of Materials Science and Engineering, Wuhan University of Technology;
2. The Institute of Technological Sciences, Wuhan University)
l.liu@whut.edu.cn

**Abstract:** In electronic packaging, electroless Ni-P coatings are normally used as diffusion barriers to retard the interfacial reactions between Cu substrates and solders. However, Ni-P coatings tend to react with solders at elevated temperature (up to 300 ℃) and form a columnar $Ni_3P$ layer containing nano pores, which badly reduces its diffusion barrier property[1,2]. Therefore, fabrications of a new diffusion barrier that can withstand high temperature are of vital importance, especially for high temperature electronics.

Electroless Ni-Fe-P coating was reported to have excellent thermal stability and excellent diffusion barrier property in electronics devices[3, 4]. However, due to the difficulties in preparations, the Ni-Fe-P coatings have not been widely used. Moreover, the effects of iron and phosphorus content on the microstructure of Ni-Fe-P coatings was not evaluated at present. In this work, the electroless Ni-Fe-P coatings with different chemical compositions were prepared using an alkaline bath with a pH of 7 to 11 on copper substrates. An orthogonal test was designed to comparatively study the effects of plating parameters on structure, morphology, and chemical compositions of electroless Ni-Fe-P coatings. The different parameters and levels of orthogonal test were outlined in attached Table 1. Then, their surface morphologies and cross-sections were observed by scanning electron microscopy (SEM). The chemical compositions of Ni-Fe-P coatings were analyzed by energy dispersive spectroscopy (EDS) incorporated with the SEM. In addition, the thermal stability of as-deposited Ni-Fe-P alloys was analyzed by differential scanning calorimetry (DSC). After annealing at various temperatures (from 300 ℃ to 500 ℃), X-ray diffractometer (XRD) provided phase transformation behavior of electroless Ni-Fe-P coatings.

Finally, electroless Ni-Fe-P coatings in varying structures (amorphous, nanocrystalline, and mixed structure) were fabricated. The surface morphologies of Ni-Fe-P coatings with different structures were shown in attached Fig.1. The results confirm that the content of phosphors plays a dominant role in controlling their structure. Moreover, the addition of iron in Ni-P alloys clearly enhanced their thermal stability and showed a potential in replacing conventional electroless Ni-P coatings in high temperature electronics.

**Keywords:** electroless Ni-Fe-P coatings, microstructure, thermal stability

**Table 1 List of $L_9(3^4)$ orthogonal test of electroless Ni-Fe-P coatings with different factors and levels**

| Levels | A/℃ | B/pH | C/($Fe^{2+}$/$Ni^{2+}$ mole ratio) |
|---|---|---|---|
| 1 | 45 | 7 | 1 |
| 2 | 60 | 9 | 3 |
| 3 | 75 | 11 | 5 |

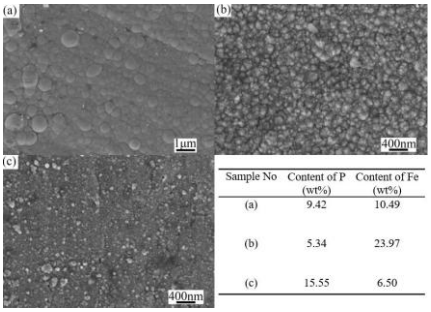


Fig.1 Surface morphologies and compositions of electroless Ni-Fe-P coatings

# Surface characterization of a selectively dissolved Ni-$Ni_3Si$ eutectic alloy

Lufeng Wei, Zhilong Zhao
(Northwestern Polytechnical University)
zhaolong@nwpu.edu.cn

**Abstract:** The lamellar porous architectures composed of alternating-remained phases and channels can be applied to fabricate multilayered devices composed of metal/ceramic- or metal/polymer-laminated architectures by injecting corresponding materials into channels. Recently, in situ $Ni_3Si$ lamellae in directionally solidified Ni-$Ni_3Si$ eutectic alloys were extracted to produce lamellar porous architectures via selective dissolution technique. The extracted $Ni_3Si$ lamellae with alternating narrow microchannels display excellent electrochemical performance and magnetic properties, which may broaden the applications of lamellar porous architecture in the fields of catalysis and magnetic multilayered devices. For optimizing the fabrication of lamellar porous architecture, an understanding of the selective dissolution behavior of α-Ni for Ni-$Ni_3Si$ eutectic alloys is urgently needed. Thus, the present work aims to investigate the selective dissolution behavior of Ni-$Ni_3Si$ eutectic alloys by using potentiodynamic polarization tests, compare the natural oxide film and the corrosion product films via X-ray photoelectron spectroscopy (XPS) analysis, and gain further insight into the mechanism of selective dissolution for dual-phase Ni-$Ni_3Si$ eutectic alloys.

Three alloys were used: α/β eutectic two-phase (Ni-11.5wt%Si), α single-phase (Ni-4wt%Si), and β single-phase (Ni-13.7wt%Si) alloys. Master ingots with these three compositions were prepared by using Ni and Si of commercial purity in a cold crucible induction furnace under argon atmosphere. The specimen was directionally solidified with a growth rate of 15 μm/s.

All electrochemical experiments were conducted in a CS350 electrochemical workstation. The specimens were used as working electrodes. The solution used for the electrochemical experiments was an aqueous electrolyte containing 2wt% ammonium sulfate, 1wt% tartaric acid, 2wt% citric acid, and 2vol% glycerol. Potentiodynamic polarization curves were obtained by sweeping the potential from –1 VSCE to 2.4 VSCE. Selective dissolution tests were performed at constant potentials of 1.1 VSCE for 20 min, 1.43 VSCE for 20 min and 1.1 VSCE for 20 h based on the polarization curves of the two single-phase alloys.

The surface of the specimen after the selective dissolution test was observed by a field emission scanning electron microscopy (FESEM) of Quanta 600FEG equipped with X-ray energy dispersive spectroscopy (EDS). The chemical states of the nickel, silicon, and oxygen on the specimen surface were analyzed using X-ray photoelectron spectroscopy (XPS; Thermo Escalab 250Xi) with Al Kα X-rays.

The α-Ni phase of the eutectic alloy was successfully removed at 1.34 and 1.67 VSHE, resulting in the formation of a channeled β-$Ni_3Si$-terminated surface. XPS analyses showed that the oxide film produced after selective dissolution was mainly composed of $SiO_2$ and Ni $(OH)_2$, with $SiO_2$ as the main component. This finding indicated that $SiO_2$ retarded the dissolution of $Ni_3Si$ phase and was preferentially formed on β-Ni3Si, resulting in successful selective dissolution. The optimum potential for selective dissolution of the α-phase was at 1.34 VSHE, at which more $SiO_2$ molecules were formed.

**Keywords:** surface characterization, selective dissolution, XPS

# Preparation of molybdenum copper composite powder by wet chemical method and its sintering properties

Chenglin Sun, Guojun Zhang
(Xi'an University of Technology)
zhangguojun@xaut.edu.cn

**Abstract:** The purpose of this study is to prepare molybdenum copper composite powders by wet chemical method, and to study the effect of sintering process and mode sintering on microstructure and properties of materials and to prepare molybdenum copper composites with excellent properties.

The experimental procedures and methods are as follows: according to the mass ratio of molybdenum and copper to 4:1, the quality of four ammonium molybdate and copper nitrate is calculated. First, the four ammonium molybdate, ammonia and deionized water are arranged into a colorless transparent solution according to the proportion of 1:1:1, then into the glass crystallization kettle and heated to the solution crystallization with an electric heating sleeve, and then slow to it. The copper nitrate solution was added and stopped heating when the solution was precipitated, and then the precursor powder of molybdenum copper was obtained by vacuum pump. In the crystallization process, the pH value of copper nitrate solution is 3, the stirring rate is 500 r/min and the heating power is 0.3 kW. The prepared precursor is then dried at 100 for 3 hours in the drying box. The precursor oxide of molybdenum copper was obtained by calcining the bulk powder at 550 for 2.5 hours. The phase, morphology and particle size of the calcined powder were analyzed by XRD, SEM and particle size distribution analyzer. The molybdenum copper composite powder was obtained by two stage reduction method in $H_2$. The first stage of reduction is reduced to 5 hours in a hydrogen atmosphere at 500, and molybdenum trioxide is reduced to two molybdenum oxide and copper oxide is reduced to copper. In the second stage reduction, the molybdenum oxide was reduced to molybdenum in the hydrogen atmosphere at 850, and the reduced product was molybdenum copper composite powder coated with molybdenum. The phase, morphology and microstructure of the powders were analyzed by XRD, SEM and TEM. When powder is pressed, the powder is put into the mould, pressed by powder pressing machine, and then pressed into a cold isostatic press to make the round billet with definite size. The preloading pressure is 32 MPa, the holding time is 3 min, the cold isostatic pressing pressure is 288 MPa, and the holding time is 10 min. Finally, the compact was sintered at vacuum temperature of 1100-1400 ℃, holding time for 2 hours, and heating rate was 10 /min.

The powder prepared by wet chemical method has uniform composition, high crystallinity, regular morphology and uniform size distribution. Molybdenum and copper exist in the form of corresponding salts, and no single other ammonium molybdate crystals exist. After hydrogen reduction, the particle size of Mo Cu composite powder is 100 nm-1 μm. By means of cold isostatic pressing, the green body with a density of about 65% can be obtained. The reduced powder can reduce the diffusion distance of the particle rearrangement in the powder, and also reduce the rearrangement resistance when the material is densified during the sintering process, which is more beneficial to the densification process of the molybdenum copper sintered body. After sintering, the block composite material with uniform microstructure, high density, good conductivity, thermal conductivity and excellent mechanical properties is obtained.

**Keywords:** wet chemical method, molybdenum copper composite

# The effect of post-weld heat treatment on the carbide evolution of Hastelloy N alloy in heat affected zone

Wanxia Wang, Chaowen Li, Li Jiang, Xiangxi Ye, Kun Yu, Shuangjian Chen, Zhijun Li, Xingtai Zhou
(Shanghai Institute of Applied Physics, Chinese Academy of Sciences)
lichaowen@sinap.ac.cn, zhouxingtai@sinap.ac.cn

**Abstract:** Hastelloy N alloy plates were welded by gas tungsten arc welding (GTAW) and then treated by post-weld heat treatment (PWHT) in order to study the carbide evolution of Hastelloy N alloy in the heat affected zone (HAZ). The results of the microstructure evolution suggest that the HAZ was divided into two parts, including eutectic zone (HAZ (E)) with width of about 400 μm near the fusion line and granular zone (HAZ (G)) with width of about 126 μm. Eutectic-like carbides can be observed in HAZ (E), while granular-like ones can be detected in HAZ (G). After PWHT, these eutectic-like carbides are spheroidized due to the remarkable decrease of the interfacial energy of these carbides. These carbides are all identified as M6C with different compositions and lattice parameters by transmission electron microscope (TEM). At the same time, the secondary carbides at the grain boundaries of the HAZ (E) become coarse after PWHT. Particularly, in the grain boundaries of the HAZ (G), little carbides were detected in the grain boundary after welding, while some secondary carbides can be observed in the grain boundary after PWHT.

**Keywords:** Hastelloy N, GTAW, post-weld heat treatment, heat affected zone, carbides

# Effect of annealing temperature on texture and magnetic properties of 6.5%Si ultra-thin strip

Siyu Zhang, Yonglin Ma, Yunpeng Zhao, Shuqing Xing
(Inner Mongolia University of Science and Technology)
164267327@qq.com

**Abstract:** Ultra-thin Silicon Strip has a wide application in power and electronics industry. In this study, a 6.5%Si ultra-thin strip with a thickness of 0.03 mm was fabricated using melt spinning method, and subsequently treated with annealing in vacuum furnace. X-ray diffraction and EBSD are employed to investigate the evolution of macro and micro texture under different annealing temperatures (880 ℃ and 920 ℃). Results show that the 6.5%Si ultra-thin strip was characterized by Cube ({001}<100>), Goss({110}<001>) and {112}<111>. After annealing, the λ-fiber remains the dominant and the grain size increases gradually with the increase of temperature. Especially, when annealed at 920 ℃, the size dominance of {001}<120> and {001}<100> grains increases gradually, and the unfavorable texture {111}<110> and {111}<112> decrease. Preeminent magnetic inductions of 1.644 T (B50) and iron losses of 5.896 W/kg (W10/400) have been achieved.

**Keywords:** 6.5%Si ultra-thin strip, microstructure, texture, magnetic properties

# Fatigue life enhancement mechanism of TB9 Hi-bolt

Qingyun Zhao
(Department of Mechanical Joining, Aeronautical Manufacturing Technology Research Institute)
zhaoqy_1997@163.com

**Abstract:** Studying on the tension-tension fatigue fracture of TB9 high strength titanium hi-bolt with SEM and EDS, the microscopic characteristics of crack initiation, crack propagation and the enhancement mechanism of fatigue life were illustrated. The fatigue fracture of this bolt is divided into fatigue crack initiation zone, crack propagation zone and instant break zone. Fatigue cracks arise from the surface and subface of bolt's head to shank fillet area, growing up with slip in initiation zone, then become the macrocracks and propagate mainly in the form of fatigue striation with some behaviors of micro-cleavage fracture. Grain boundary αand dislocation in secondaryα-phase and grain boundary has a significant influence on fatigue crack initiation. The existance of worked layer is benefit for fatigue life.
**Keywords:** TB9, fatigue fracture

# Evaluation method of fatigue life based on damage mechanics

Yajun Zhang
(Luoyang Ship Material Research Institute)
zhangyj309@163.com

**Abstract:** Based on Miner linear cumulative damage theory and basic idea of damage mechanics, critical fatigue damage parameter Dc of 10CrNiMo steel was attained by taking smooth plate specimens in a test with an assumed load spectrum under cantilever bend loading. Pertinence of fatigue damage amount and its corresponding microscopically measureable parameter, the displacement of loaded point of the specimen was investigated and the relation of them was built, through which fatigue damage amount of metallic materials could be measured indirectly by inspecting change of displacement at loaded point. According to approaching-degree of fatigue damage amount to critical fatigue damage value, fatigue life of metallic materials could be evaluated and the evaluation results could provide reference for safe service and remaining life evaluation of metallic materials in view of damage mechanics.
**Keywords:** cantilever bend loading, critical fatigue damage parameter, fatigue damage amount, fatigue life evaluation

# Microstructure and mechanical property of Al/SiCp nanocomposite coating produced by cold spraying of ball-milled powder

Hongtao Wang, Hailong Yao, Xiaobo Bai, Qinyu Chen, Chao Yang, Gangchang Ji
(Jiujiang University)
wanght7610@163.com

**Abstract:** Al-based nanocomposite coating reinforced with silicon carbide (SiC) particles have a unique set of properties for weight-sensitive applications in the transport sector such as cylinders, pistons, brake rotors, etc. because of their high specific strength and improved wear resistance. In this paper, Al-based nanocomposite coatings reinforced with different volume fraction of SiCp particles (20%-60%vol) were produced by cold spraying of ballmilled Al/SiCp composite feedstock powder. The microstructure characteristics of ballmilled Al/SiCp composite powder and cold-sprayed coatings were examined by optical microscopy (OM), scanning electron microscopy (SEM) and X-ray diffraction analysis (XRD). The Mechanical property of Al/SiCp nanocomposite coatings such as microhardness and wear resistance were investigated and the wear mechanisms were discussed based on worn surfaces examinations.
**Keywords:** Al/SiC nanocomposite, cold spraying, ball milling, microstructure, mechanical property

# Phase transformation and irradiation effects of BN/BAS ceramic composites induced by charged argon ion beam

Qian Li[1], Bo Zeng[2], Zhihua Yang[1], Dechang Jia[1], Xiaodong Zhang[3], Yu Zhou[3]
(1. Institute for Advanced Ceramics, Harbin Institute of Technology;
2. Material Science and Engineering School, Harbin Institute of Technology;
3. School of Materials Science and Engineering, Harbin Institute of Technology)
zhangxiaodong@hit.edu.cn

**Abstract:** Barium alumino silicate (BAS), particularly in its monoclinic form, has potential as matrix material for ceramic matrix composites used at high temperatures, due to their high oxidation resistance, low and linear dielectric constant, and low coefficient of thermal expansion. Composite are usually used to be wave-transmitting materials used in radome exposed to intense fluxes of ions and electrons from complicated space environment. Irradiation has vital effect on the spacecraft materials about cavities, lattice parameters and others microstructure defect which have decisive role in proper functioning of spacecraft. Therefore, it is certainly worth characterizing the composite materials irradiated by ions beam. In this paper, BAS-BN composite ceramics were synthesized by hot-pressing sintering at 1500 ℃ with h-BN content at 10%, 30% and 50wt%. Composite ceramics was irradiated by 70, 110 and 150 keV $Ar^+$ at room temperature with fluence $1\times10^{16}$ $cm^{-2}$. X-ray diffraction measurements revealed that following irradiation with $Ar^+$ ions, in the 30% BN-BAS composite the hexagonal phase was gradually replaced by monoclinic phase. Transmission electron microscopy (TEM) experiments indicated that in a sample irradiated by Ar ions the transformed composite possesses a more monoclinic than hexagonal celsian. Surface modification by different energy ions implanted was investigated by X-ray photoelectron spectroscopy (XPS) which showed the decomposition of Si-O or Al-O band in the $[Si(Al)O_4]$ tetrahedral. Grazing incidence X-ray experimental were needed to prove the phase transformation. On the basis of the experimental results, the mechanism of phase transformation and surface modification was discussed.
**Keywords:** BAS-BN ceramics, surface modification, ions beam implantation, irradiation effects, phase transformation

# Effect of tempering temperature on low carbon bainite steel plate

Yongda Yang[1], Yanfeng Wang[1], Guobiao Di[1], Changwen Ma[1], Qingshen Ma[1],
Chengliang Han[2], Dongli Meng[2]
(1. Shougang Group Co., Ltd. Research Institute of Technology;
2. Qinhuangdao Shouqin Metal materials Co., Ltd.)
526026821@qq.com

**Abstract:** The effect of tempering temperature on the microstructure and mechanical properties of low carbon bainite steel plate produced by TMCP process was investigated. All samples were cut from the same steel plate with thickness of 40 mm, and then tempered at temperature ranging from 300 ℃ and 700 ℃ for 120 min. The microstructures were studied using optical microscope and transmission electron microscope. The results are shown as follows. For samples tempered not higher than 600 ℃, both of the yield strength and tensile strength increased due to the enhanced precipitation strengthening effect by Nb/Ti carbides with higher tempering temperature, while the elongation and impact energy don't change obviously. Moreover, the matrix consisting of acicular ferrite and granular bainite shows great microstructural stability when the temperature increases. When the tempering temperature increased to 700 ℃,the strength and impact energy decreased greatly, for reason of the coalescence of substructures and the coarsening of Nb/Ti carbides.

**Keywords:** bainite steel, tempering temperature, strength, precipitation, impact energy

# Influence of ferrite content and tempering temperature on the mechanical properties of HSLA steel

Hao Yu, Shaoyang Wang
(University of Science and Technology Beijing)
yuhao@ustb.edu.cn

**Abstract:** The effect of ferrite content on the microstructure and mechanical properties evolution of high strength low alloy (HSLA) steel tempered at different temperatures was studied. The hot rolled HSLA steel specimens were quenched from the range of 790-900 ℃ to obtain >40vol% martensite and then tempered at 180 ℃ and 450 ℃, respectively. Microstructure analysis revealed that with the increase of quenching temperature the ferrite content reduced and only martensite exists after quenched from 900 ℃, and this introduced more dislocations into the microstructures. The tempering mainly affected the strength difference between ferrite and martensite to change the mechanical properties of the specimens. The yield and tensile strength increased with the decrease of ferrite fraction after tempered and the tensile strength was lower tempered at 450 ℃ than that tempered at 180 ℃. While this is not the change for the yield strength which was determined by the ferrite yield strength and had the higher values tempered at 450 ℃ when the ferrite is over 26vol% or by the martensite yield strength and had the higher values tempered at 180 ℃ when the ferrite is less than 3vol%. The total elongation increases with the increasing ferrite content tempered at both temperatures. The variations of the impact energy with the ferrite content tempered at 180 ℃ and 450 ℃ are contrary. But they all have good impact energies with complete martensite.

**Keywords:** ferrite content, martensite, tempering temperature, tensile property, impact property

# CCT curves and microstructure of a new type bainitic wear-resistant casting steel

Bo Hu, Xianjun Li, Wenliang Zhang, Junjie Liu, Ping Luo, Kun Deng
(Beijing Research Institute of Mechanical & Electrical Technology)
18811795072@163.com

**Abstract:** In order to provide the guidance to actual production, the continue cooling transformation (CCT) curves of a new type bainitic wear-resistant casting steel were determined by the method of dilatometric change, combining with metallographic and microhardness examinations. The microstructures after cooling at different cooling rates were investigated with optical microscope; the microhardness and the effect of alloy elements were analyzed. The results indicated that the starting temperature of bainite and martensite are obviously decreased to about 456 ℃ and 303 ℃, respectively. Critical cooling rate is between 15 ℃/s and 30 ℃/s. Ferrite and pearlite with microhardness of 263 HV can be reaped with the cooling rate of 0.05 ℃/s; when the cooling rate is 0.1 ℃/s, ferrite, pearlite and bainite are received. However, bainite/martensite multiphase microstructures whose microhardness is 520-585 HV are obtained with the cooling rate range of 0.25-15 ℃/s. With the cooling rate increasing to 30 ℃/s, the microstructure becomes all martensite and microhardness reaches 592-596 HV. As a result of alloy elements (such as Mo, Cr, Mn), the hardenability of the steel is significantly good and bainite/martensite multiphase microstructures can be obtained under the condition of air cooling, which is very environment-friendly and convenient for actual production.

**Keywords:** bainitic wear-resistant steel, CCT curves, microstructure, microhardness

# Effect of quenching temperature on the microstructure and corrosion behavior of X80 pipeline steel

Jing Ma[1], Haifeng Chen[1], Fan Feng[1], Lifeng Fan[2]
(1. Hebei University of Science and Technology; 2. Inner Mongolia University)
majingt@qq.com, ysufanlifeng@foxmail.com

**Abstract:** X80 pipeline steel was quenched at 760, 740, 720, 700 and 680 ℃ respectively to obtain different amounts of bainite and ferrite phases. The microstructures, hardness and polarization behaviors in 3.5wt%NaCl solution were investigated. The results show that with the decrease of quenching temperature, the amount of polygon ferrite (PF) was increased while those of acicular ferrite (AF) and bainite phases were decreased. Moreover, grain size was increased and the hardness was decreased. The corrosion potentials of X80 steel quenched at lower temperature were more positive and corrosion current densities are lower, which indicates the X80 steel with more ferrite phase have excellent corrosion resistance. The reasons are as follows: 1) the larger grain size have less grain boundaries; 2) ferrite is a single phase solid solution while bainite is a two-phase structure so that more ferrite means better corrosion resistance. However, the quenching temperature cannot be selected too low according to the requirement of mechanical properties. The appropriate quenching temperature is 720 ℃ for comprehensive consideration of corrosion resistance and mechanical properties.

**Keywords:** X80 pipeline steel, quenching temperature, microstructure, corrosion behavior

# Microstructure and mechanical properties of uranium alloy impacted by steel projectile under different velocities

Dongli Zou, Lifeng He, Dawu Xiao, Zhicong Qiu
(Institute of Materials, China Academy of Engineering Physics)
donglizou@126.com

**Abstract:** Deformed microstructure and mechanical properties of uranium alloy impacted by steel projectile at the velocity ranged from 10 m/s to 90 m/s was investigated. The spherical cap craters were formed in uranium alloy targets impacted by steel projectile, and the crater diameter and depth were varied linearly with impact velocities. At a velocity of 90 m/s, the diameter and depth of the impacted crater were 6.29 and 1.67 mm, respectively. Microstructural observation shows that twinning was considered as a dominant plastic deformation mechanism of depleted uranium subjected to impact loadings, and the twins {130} and {172} were distinguished and confirmed. Microhardness measurement shows that the microhardness value adjacent to crater was much higher than that of the matrix.

**Keywords:** uranium alloy, dynamic deformation

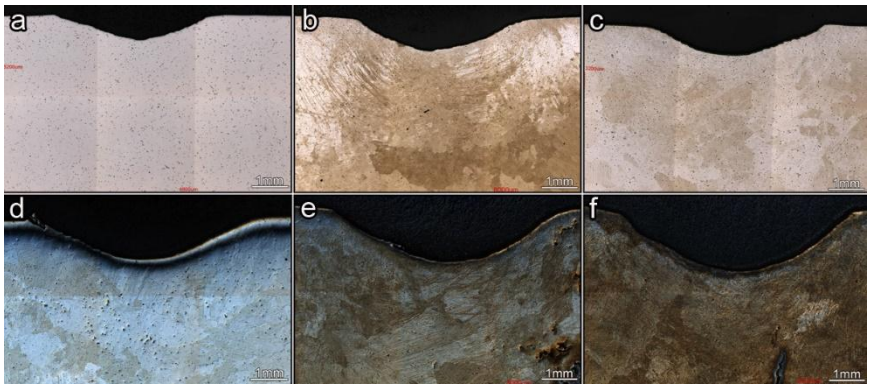


Fig.1 Crater cross-section views of metallic uranium under different impact velocities: (a) 10 m/s; (b) 20 m/s; (c) 30 m/s; (d) 50 m/s; (e) 70 m/s; (f) 90 m/s

# Effect of annealing temperature on the microstructure and mechanical properties of the ferrtic rolling low carbon steel sheet

Hu Zhao[1], Pengfei Cheng[2], Jiangong Wang[2], Xiaodong Wang[2]
(1. Research Institute of Technology, Shougang Group; 2. Shougang Jingtang United Iron & Steel Co., Ltd.)
zhaohuf@163.com

**Abstract:** The microstructure characteristic of hot-rolling low carbon steel plate produced by ferritic rolling process and normal rolling process was comparatively investigated. The microstructure of the ferritic rolling plate along the thickness direction was inhomogeneous with fully recrystallized grains in the surface layer and partially recrystallized grains in the center layer. The microstructure evolution during annealing of the low carbon steel sheet after pickled and cold rolled was analyzed. The higher annealing temperature improved the formability of the steel sheet. In addition, the microstructure differences of the annealed low carbon steel produced by ferritic rolling process and normal rolling process were discussed.

**Keywords:** Ferritic rolling, recrystallization, texture, grain size

# The effect of precipitation on the property of high strength steel plates under different heat treatment techniques

Yanqiu Fan
(Shougang limited corporation Research institute of technology)
fanyanqiu8807@163.com

**Abstract:** As we know, high strength steels not only should have high strength, but also should have good ductility and toughness. In view of this fact, it is necessary to develop high strength steels with high strength and good toughness. In addition to the content of carbon and alloy element, precipitation is also an important role in achieving excellent properties. In this paper, we have studied the effect of precipitation on the property of high strength steel plates under different heat treatment techniques. The tentative steel plates, after TMCP, were tempered at four different tempered temperature, 500, 550, 600 and 650 ℃. The mechanical properties of steel tempered at various temperatures were carefully examined, and the precipitation, especially nanoscale ε-Cu precipitates, were systematically investigated using transmission electron microscope. The results showed that the microstructure was mainly bainite, and there was an increase and then a decrease in strength and it reached its peak at 600 ℃ , which was attributed to the precipitation characteristics of precipitates. Furthermore, numerous uniformly dispersed nanoscale ε-Cu precipitates enable the steel plates tempered at 600 ℃ to obtain the combination of high strength and excellent toughness.

**Keywords:** precipitation, high strength steel plates, temperature

# Investigations of the tensile properties and fracture characteristics of amorphous ribbons Fe81.50B1.40Si7.95Nb7.37Cu1.728 alloy

Sheng Lei
(Anhui University)
leish1964@vip.126.com

**Abstract:** A number of Fe-Si-B amorphous ribbons were made by the melt-spun method. The microstructure, the mechanical and other relevant properties of thin amorphous ribbons of Fe81.50B1.40 Si7.95Nb7.37Cu1.728 alloy at room temperature were studied using many equipment including differential scanning calorimetry (DSC), X-ray diffraction (XRD), scanning electron microscope (SEM) and tensile machine. Significant different microstructure exists between the free and wheel face of the thin amorphous ribbons. The free face is smooth while the wheel face is coarse with a great number of micro voids on the surface. Experimental results show that the tensile strength and elastic modulus of the thin amorphous ribbons at room temperature are found to be 1951 MPa and 70 GPa, respectively. The fracture appearance of amorphous ribbons of Fe81.50B1.40Si7.95Nb7.37Cu1.728 alloy is a mixed mode of ductile and brittle fracture which includes dimples and partial cleavage or quasi-cleavage fracture. The dimple feature proves that it still has plastic characteristics on the micro scale.

**Keywords:** amorphous alloys, tensile strength, ductile, brittle fracture

# Several methods of reducing the testing errors in rockwell hardness

Chunchen Yao[1], Menglin Wang[2], Yingying Ruan[3], Xuemin Lv[4], Zheming Yang[3]
(1. Jiangnan Industries Group Co., Ltd.;
2. School of Foreign Languages, Beijing Technology and Business University;
3. Jiangnan Industries Group Co., Ltd.; 4. China Aviation Research Institute of Hunan Power Machinery)
yaocc112@163.com

**Abstract:** In order to reduce the testing errors in Rockwell hardness of metal specimens, apart from testing strictly according to GB/T 230 and other relevant inspection specifications, several methods had been tried out and examined: firstly, correct the hardness of testing pieces directly by using the hardness reference blocks to calibrate the hardness tester; secondly, correct the hardness of testing pieces by linear calculation on the errors in different hardness values to calibrate the hardness tester; and as to a large number of testing pieces, check the hardness twice among which the second time is in a reverse order. The trials show that these methods are effective ways to further improve the testing accuracy of Rockwell hardness.

**Keywords:** metal material, physical and chemical testing, rockwell hardness, error correction

# Evolution of microstructure and strain-induced precipitates in Nb-Ti extra heavy slab during hot-core heavy reduction rolling

Meina Gong, Haijun Li, Bin Wang, Zhaodong Wang
(The State Key Laboratory of Rolling and Automation, Northeastern University, Shenyang, China)
lihj@ral.neu.edu.cn

**Abstract:** Thermal-mechanical simulation experiments have been conducted to study effect of niobium and titanium carbonitrides precipitation during hot-core heavy reduction rolling by Gleeble-3800. The effect of deformation parameters on precipitates morphology of Nb–Ti micro-alloyed slab was studied by two-stage interrupted compression testing. The result showed that carbonitrides precipitates formed at dislocations, sub-boundaries, and grain boundaries by strain. These strain-induced precipitates significantly suppressed recrystallized grain nucleating and growing. Compared quantification of driving force and pinning force, recrystallization would not be completely suppressed by the pinning force.

**Keywords:** hot-rolling deformation, strain-induced precipitates, pinning force, driving force

# Microstructure and mechanical properties of in situ Mo/$Mo_2C$ composite

Xuan Chen
(Xi'an University of Technology)
15929894073@163.com

**Abstract:** Molybdenum (Mo) is a kind of promising refractory metal material because of its attractive comprehensive properties including the relatively high melting temperature of 2610 ℃, creep resistance, low thermal expansion coefficient, excellent electrical conductivity and corrosion resistance. Therefore, the alloys based on Mo possess prospects for wide applications such as in casting mould, rocket nozzle and combustor. However, its limited strength and poor machinable properties also restrict the development of applications at elevated and ultrahigh temperature. Thus, the strengthening and toughening of Mo alloys has attracted lots attention. The molybdenum carbide has very attractive properties such as high melting temperature, high hardness, high thermal stability and mechanical stability, which can act as strengthening phase for improving mechanical properties of molybdenum alloys. It is also a potential grain refiner in the Mo alloys. In-situ composites offer good properties as the particles are formed within the matrix melt. The particle formation is also uniform and establishes good interface bonding between matrix and reinforcement material. Therefore, the two dimensional graphene was chosen as raw material. The calculated quantities of graphene powder was added into Mo powder via solid-solid doping method followed by vacuum hot-press sintering to produce Mo composite reinforced by 15wt% $Mo_2C$. According to the available literatures, the vacuum hot-press sintering (HP) can efficiently accelerate the densification of samples which is beneficial to fabricate highly compact alloy blocks with fine grains under the condition of less molding pressure and shorter sinter time. Solid-solid doping was done using a planetary ball mill equipped with agate pot and balls to help the dispersion of graphene which reacted with Mo and produced $Mo_2C$ during the sintering. The formation of hexagonal and orthorhombic $Mo_2C$ particles were confirmed from X-ray diffraction pattern and selected area electron diffraction. Transmission microscopy (TEM) analysis revealed that micron and submicron $Mo_2C$ particles were mainly distributed at the Mo grain boundaries. For the sinters, the grain size of Mo/$Mo_2C$ composite was greatly decreased by 50 % compared with the pure Mo. Meanwhile Mo/$Mo_2C$ composite with higher relative density were obtained. The test results of mechanical properties indicated that the yield strength and hardness at room temperature of composite have improved 94 % and 35 %, respectively. Compression tests were performed using the Gleeble 3800 testing machine between 1000 ℃ and 1100 ℃ at 0.001 mm/s compression strain rate and the results showed that the yield strength at 1000 ℃ and 1100 ℃ of Mo/$Mo_2C$ composite were increased by 106% and 185%, respectively, compared with the pure Mo. Microstructure of pure Mo and Mo/$Mo_2C$ composite after compressing was characterized by scanning electron microscopy and TEM. The effects of $Mo_2C$ on the high temperature deformation behavior and microstructure evolution of the Mo/$Mo_2C$ composite were analyzed. The strengthening effect of Mo/$Mo_2C$ composite can be divided into two parts: the grain refining strengthening caused by the formation of $Mo_2C$ and the Orowan strengthening effect of $Mo_2C$ working as reinforcements. The quantitative relationships between the yield strength and the size, volume fraction of $Mo_2C$ particles and Mo grain size were presented.

**Keywords:** Mo composite, $Mo_2C$, mechanical properties

# Influence of Si/B ratio on microstructural evolution and properties of ultrafine-grained Mo-$Mo_3Si$-$Mo_5SiB_2$ alloys doped with $La_2O_3$

Rui Li
(Xi'an University of Technology)
maoruiruimail@sina.com

**Abstract:** Structural materials used in high-temperature environment should have adequate strength, creep and oxidation resistance. Also, acceptable fracture toughness at room temperature is necessary. Since Nickel based superalloys are approaching their maximum application temperature limited of 1150 ℃, Mo-Si-B alloys with high melting points for the service at or above 1250 ℃ have been the focus of widespread interest. The Mo-Si-B alloys of α-Mo-$Mo_3Si$-T2 system which potentially meet the requirements of an acceptable balance between creep and oxidation resistance at high temperatures and fracture toughness at room temperature are more suitable for applying in the field of engineering and industry. In order to investigate the effect of the Si/B ratio on the microstructure evolution, mechanical properties and oxidation behaviors, 0.9wt% $La_2O_3$ doped Mo-Si-B alloys with Si/B ratios of 2.4, 1.4 and 0.7 were prepared by mechanical alloying (MA) and hot pressing (HP) sintering technology corresponding to the nomial compositions of Mo-12Si-5B, Mo12Si-8.5B and Mo-12Si-17B alloys, respectively. These three alloys mainly consisted of αMo, $Mo_3Si$ and $Mo_5SiB_2$ phases and exhibited typical multi-scale microstructure. The intermetallic phases ($Mo_3Si$/$Mo_5SiB_2$) maintained sub-micron scale range and the α-Mo ductile phase was in the range of submicro to micro-scale. Besides, the nano-scale $La_2O_3$ particles were located at the grain boundaries and partially in the grain interiors. The alloys with Si/B ratios of 2.4 and 1.4 (≥46vol% of α-Mo phase) possessed a continuous α-Mo matrix where $Mo_3Si$/$Mo_5SiB_2$ particles distributed dispersedly. The former (Si/B=2.4) demonstrated excellent fracture toughness values of 9.8 MPa $m^{1/2}$ and 12.3 MPa $m^{1/2}$, which were determined from single edge notch bend tests and indentation tests, respectively. As decreasing the Si/B ratio, the fracture toughness of alloys decreased. Based on theoretical analysis, higher α-Mo phases volume fraction provided remarkable improvement in fracture toughness primarily by promoting crack trapping mechanism. Besides, $Mo_3Si$/T2 particles elevated cracks deflection and interfacial debonding effects, which provided further resistance to cracks growth. The alloy with Si/B ratio of 0.7 (≥71vol% of intermetallic phase) formed a continuous intermetallic matrix with embedded islands of α-Mo phase, exhibiting the highest compression strengths of 1979 MPa (800 ℃), 1837 MPa (1000 ℃), 1211 MPa (1200 ℃) and 646 MPa (1300 ℃), respectively. Switching from a α-Mo matrix to an intermetallic matrix resulted in a significant increase of the compression strength. At even higher temperatures between 1200 ℃ and 1300 ℃, the strengthening contribution of intermetallic matrix becomes more prominent. During isothermal oxidation tests at 1000 ℃ in static air, the alloy with Si/B ratio of 2.4 exhibited a heavy mass loss in initial transient stage. The duration of the transient stage was about 2 h. In contrast, alloy with Si/B ratio of 0.7 showed a minimal mass loss and duration of 15 min. Lower Si/B ratio promoted a continuous borosilicate scale quickly covering the entire alloy surface during the transient stage. Besides, it improved the protectiveness and density of the borosilicate scale in the steady stage, which effectively restricted the inward diffusion of oxygen and decreased the thickness of the inner $MoO_2$ layer and the inner oxidation zone (IOZ).

**Keywords:** Mo-Si-B alloys, Si/B ratio, microstructure, mechanical properties, oxidation performance

# Improvement of fracture toughness in Mo-Si-B alloy with a microstructure of bimodal α-Mo phase

Wang Juan
(Xi'an University of Technology)
sxwj@163.com

**Abstract:** Mo-Si-B alloys in the ternary phase field are identified as promising high temperature structural alloys for use at higher temperatures by offering interesting mechanical and oxidation properties in comparison with Ni-based superalloys. Mo-12Si-8.5B (at%) alloy possess a continuous α-Mo matrix with intermetallic particles uniformly dispersed in the matrix microstructure showing a promising balance between mechanical properties and oxidation resistance by containing an appropriate volume fraction of intermetallic compounds and the a-Mo solid solution phase. Intermetallic phases are used for high temperature properties and a ductile Mo phase for fracture toughness. The alloys generally possess a good oxidation resistance around 1400 ℃, where a continuous coverage of borosilicate glass is established with a low diffusivity for oxygen. Still the key issue continues to be the fracture toughness. The goal of this research is to fabricate ultrafine-grained Mo-Si-B powders with coarse Mo-Si-B powders, and mix them in order to create a microstructure consisting of intermetallic phases bonded by a continuous matrix of bimodal a-Mo. It is reported that development of bimodal grain structure (i.e. mixed coarse and fine-grain structure) is a useful concept of improving the ductility of ultra-fine grains metals and alloys. However, such microstructure shows excellent combination of strength and ductility owing to the high strain-hardening capacity of the coarse-grains and strengthening ability of the ultra-fine grains. Bimodal grain structures, on the other hand, enhances the ductility and fracture toughness of these alloys through in situ ductile-phase toughening. In addition, the resulting crack bridging and plastic deformation of the particles, together with crack deflection and interfacial debonding, provide the main contributions to toughness. In the present work, Mo-12Si-8.5B-1.0wt%$ZrB_2$ alloys consisting of three phases of $Mo_5SiB_2$ (T2), $Mo_3Si$ and Mo solid solution (α-Mo) were prepared by mechanical alloying following hot pressing. In order to fabricate the Mo-Si-B alloy with bimodal α-Mo phase, the Mo-Si-B powders mechanically-milled for 20 h were mixed with the original mixed Mo-Si-B powders to sinter. The alloys exhibited a microstructure consisting of intermetallic phases bonded by a continuous matrix of α-Mo that showed the a mixed bimodal microstructure composed of predominant ultrafine α-Mo with nanoscale and a small quantity of microscale α-Mo grains, and the corresponding α-Mo phase size distributions plotted in terms of the area-frequency histograms showed the presence of two-separate peaks. Since the coarse-Mo phase is thought to enhance toughness by forcing the crack to interact with the -Mo phase, consequently, if the crack can be arrested at the ductile phase such that it must renucleate, on the other side, the resultant crack trapping acts to toughen the material intrinsically, as schematically. However, the existence of fined-grains (T2 and $Mo_3Si$) in the bimodal alloy provide the main contributions to the compressive strength. The fracture toughness obtained from testing of the bimodal sample had been found to be in the range of 13.44-13.71 MPa $m^{1/2,}$ showing an improvement of 48.34%-51.32% compared with the ultra-fined MSB alloys. Simultaneously, the compressive strength of the bimodal alloy showing 2856.1 MPa, maintained the same high level compared with ultra-fined MSB alloy.

**Keywords:** Mo-12Si-8.5B alloy, bimodal microstructure, fracture toughness

# Effect of austempering process on the microstructure and properties of D2 cold work die steel

Jianbo Liu, Xuebin Zhang, Kexing Song
(School of Materials Science and Engineering, Henan University of Science and Technology)
13849903660@163.com

**Abstract:** D2 cold work die steel has much poor impact toughness. However, many investigations demonstrate that martensite/bainite (M/B) duplex microstructure with an amount of lower bainite can improve effectively the impact toughness of tool/die steel. So this paper investigated the effect of austempering process on the hardness, impact toughness, microstructures and fracture morphology of D2 cold work die steel. The specimens were austenitized at 1030 ℃ for 30 minutes, and quenched in 270 ℃ salt bath for 0, 1, 2, 4 and 6 hours, then quenched in oil cooling to room temperature, finally tempering at 200 ℃ for 2 hours, obtained martensite/bainite (M/B) duplex microstructure with different amounts of lower bainite. The hardness and impact toughness of specimens have been determined, the microstructures and fracture morphology have been characterized by OM, SEM coupled with EDS and XRD. The obtained experimental results and their pertinent analyses are as follows:

(i) The hardness and impact toughness test results show that the hardness first increases and then decreases and the impact toughness increases gradually with the increase of salt bath holding time. Generally speaking, the quenched in 270 ℃ salt bath for 0 hour can be regarded as conventional heat treatment (CHT).When the salt bath holding time is 2 hours, the hardness increases by 0.4 HRC up to 61.9 HRC and the impact toughness increased by 31.6% up to 48.7 J/cm$^{-2}$ compared with the ones of CHT, respectively. Considering the actual working conditions of D2 cold work molds, the process of quenched in 270 ℃ salt bath for 2 hours can be regarded as the optimum austempering process.

(ii) The microstructure examinations show that there are many alloy carbide particles which size and distribution are asymmetrical in the matrix. EDS tests show that the large-size particles (>5 μm) are primary alloy carbides which enrich alloy elements Cr, Mo, and V, but the small-size particles (<5 μm) are secondary alloy carbides which enrich Fe element. With the austempering, the lower bainite transformed previously segments the original austenite grain, the effective grain size of the austenite reduces obviously, and then the acicular martensite produced by the oil quenching is smaller and finer. The ferrite grains can improve effectively the mechanical properties of material. X-ray diffraction line profiles exist the (200) peak of austenite. Currently, the matrix is composed of M/B duplex microstructure with different amounts of lower bainite, a few of retained austenite and a little of alloy carbide particles.

(iii) SEM micrographs of fractured surfaces show that the matrix exhibits quasi-cleavage fracture mechanism and accompanies a few of shallow and small dimples, whereas the fracture morphology of (M/B) duplex microstructure contains more cleavage steps and tear marks. There are more fine and narrow cleavage facets on the fracture with the presence of lower bainite. With the increase of salt bath holding time, the amount of lower bainite increases, which can further relieve the stress concentration of the crack tip and reduce the speed of crack propagation, then the intergranular fracture is rapidly reduced. Respectively, the following transformed acicular martensite is effectively refined, which can lead to that the unit crack path is reduced and the quasi-cleaving surfaces are more, tinier and smaller. Finally, the fracture toughness is greatly improved.

**Keywords:** D2 cold work die steel, austempering, hardness and impact toughness, martensite/bainite (M/B) duplex microstructure, fracture morphology

# Effect of heat treatment parameters on microstructure and mechanical properties of a modified AISI 4140 steel

Xiaoyang Song[1], Yuqing Liu[2], Xinjin Zhang[1], Xuejiao Zhang[1], Zhizhong Dong[3], Lin Zhu[1]
(1. National Eng. R&D Center for Heavy Machinery Technologies, Tianjin Heavy Industries Research & Development Co., Ltd.;
2. Shandong Special Equipment Inspection Institute Co., Ltd;
3. School of Materials Science and Engineering, Tianjin University of Technology)
zhizhong_dong@126.com, zl508@126.com

**Abstract:** The microstructural and mechanical properties of a modified AISI 4140 steel with different heat treatment parameters have been investigated in this paper. The effects of heat treatment temperature on the grain size, microstructure and mechanical properties were discussed respectively. The microstructure characteristics with different tempering temperature were carefully examined by optical microscopy (OM), scanning electron microscopy (SEM). Transmission electron microscopy (TEM) observation and selected area electron diffraction (SAED) analysis were performed to analyze the type, size and morphology of carbides. Besides, the hardness, tensile property, impact toughness of the modified AISI 4140 steel was also evaluated.

The experimental results indicated that the average grain size kept almost stable about 14 μm with the increase of normalizing temperature, after the normalizing process with the temperature of 850-900 ℃. However, it happened to an obvious increase of the average grain size over 20 μm, with the normalizing temperature up to 925 ℃, which may lead to the reduction of mechanical properties. The martensite hardness presented an increase followed by a drop-down as the normalizing temperature increased, and it can reach the maximum value of 457 HV10 at 880 ℃.

The tempered microstructure of the modified AISI 4140 steel possessed the typical tempered martensite with plenty of precipitations. TEM results showed that the precipitations consisted of mainly the needle-like $M_3C$ and granular $M_7C_3$ carbides. In addition, a little of ultra-fine V-rich MC carbides was often observed in the steel due to the vanadium addition. The $M_3C$ carbide size becomes shorter and thicker with more carbides precipitate and growing up, as the tempering temperature increases to 640 ℃.

It was well established that the microstructure during heat treatment strongly influenced mechanical and physical properties. With the increase of tempering temperature in the range of 580-640 ℃, the yield strength dropped down from 1044 to 855 MPa, while the low-temperature impact toughness (–18 ℃) increased from 55 to 108 J, because of the lower dislocation density and more precipitations. An empirical linear expression between yield strength and tempering parameter of the modified AISI 4140 steel was established.

The obtained expression was fitted as $\sigma_s$=4798–0.24 $T$(14.4+lg$t$).

The different microstructure of the modified AISI 4140 steel conduced to different mechanical properties in the steel. In comparison to the microstructure using the relatively low tempering temperature, the tempered martensite with the shorter and thicker $M_3C$ carbide and more precipitated phases at higher tempering temperature was beneficial to ductility and low-temperature impact toughness but led to lower hardness and strength. These results provided the further possibility of optimizing the heat treatment parameters to control the microstructure and obtain desirable mechanical performance.

**Keywords:** microstructure, carbide, mechanical property, toughness, AISI 4140, heat treatment parameters

# Production and characterization of vermicular graphite steel with 2% carbon

Gustavo Satoru Takeya[1], José Benedito Tosoni Decarlis N. Rodrigues[2], Amadeu N. Lombardi[3], George E. Totten[4], Luiz Carlos Casteletti[1]
(1. São Carlos School of Engineering, EESC-USP; 2. Baldan Implementos Agrícolas; 3. Federal Technological University of Parana UTFPR; 4. Portland State University)
gutakeya@yahoo.com.br

**Abstract:** Vermicular cast iron (also called compact cast iron) have long been considered flaws in the cast iron modularization process. The first reports about this material were made in the 1940s, and from the 1960s the first patents appeared. In terms of properties, these vermicular cast irons presents intermediate characteristics between gray cast iron (low mechanical strength but high thermal conductivity) and nodular cast irons (high mechanical strength and low thermal conductivity). They are also economically competitive because they admit a higher amount of sulfur than nodular cast irons, do not require long cycles of heat treatment such as malleable cast irons and a casting that produces nodular molten irons can also produce the vermicular cast iron. They also have a good vibrations and sound damping rates and impact-absorbing capacity similar to that of ductile cast irons. Its uses include brake discs, pump housings, brackets, diesel engine blocks. Many methods of obtaining this cast iron have been developed over the years, such as the use of a smaller amount of Mg than that used in the production of ductile cast irons; combined treatment of Mg and anti-spheroidization elements, such as titanium or aluminum; use of zirconium, lead or tin; or blowing of gases such as methane, argon, acetylene, heated in the molten metal already treated with magnesium. The mechanical properties of this material can be improved by means of thermal treatments of austenome, which produce a microstructure called ausferrite, formed by acicular ferrite and retained austenite of high carbon instead of martensite as in a conventional quenching. This microstructure presents good mechanical resistance and low distortion when compared to that obtained in the quenching, which allows the fabrication of near net shape parts, considerably reducing process costs. It should be avoided that this ausferrite does not become bainite, since its preparation involves heating the material to a temperature of austenitization and subsequent cooling in the range of 300 ℃ to 500 ℃, depending on the chemical composition. The material is maintained at this temperature until its microstructure becomes ausferrite, but when a certain time is exceeded, this ausferrite decomposes into bainite. In the present work, a steel with a vermicular structure was obtained using Fe-Si-Ca as a nodularization agent. This steel contains carbon at about 2wt%, which is an intermediate value between traditional graphite steels (1.0wt%) and ductile cast irons (2.3-3.7wt%) and niobium was added at 0.5wt%. Niobium is known as a steel grain refiner and produce hard carbides when used in greater amounts. Optical microscopy, SEM, X-ray diffraction, Vickers microhardness, tensile and Charpy type impact tests and calotest type wear tests were used to characterize the materials produced. Austempering treatment was successful, producing a material with mechanical properties superior to that the material in the as-cast condition. In comparison with an alloy without the addition of niobium, the microstructure was more refined and with a lower graphite content, indicating that part of the Nb formed hard carbides in the matrix, which explains the increase in hardness and wear resistance of this alloy with niobium.

**Keywords:** vermicular steel, production, austempering, niobium

# Obtaining the TTT diagrams for graphitic steels alloyed with niobium

Carlos Alberto Soufen[1], Gustavo Satoru Takeya[2], Amadeu N. Lombardi[3],
Luiz Carlos Casteletti[2], George E. Totten[4]
(1. Universidade Estadual Paulista "Júlio de Mesquita Filho", UNESP–Bauru;
2. São Carlos School of Engineering, EESC-USP;
3. Ederal Technological University of Parana–UTFPR; 4. Portland State University)
gutakeya@yahoo.com.br

**Abstract:** The good combinations of mechanical properties of austempered spheroidal graphite cast steel (AGS), combined with the development of modern casting techniques, have resulted in a very promising technical and economical product. Compared to AGS, the austempered nodular cast irons (ADI) have good mechanical properties, but their Young's modulus is in the range of 160 to 170 GPa, approximately 20% less than conventional steels, thus the development of AGS was aimed at obtaining a new material with mechanical properties superior to those of ADI but with the advantages of ADI in relation to conventional cast steel such as lower production cost, higher wear resistance and vibration damping capability. Its carbon content is almost a third of that present in the ADI, which results in a lower graphite volume, with the consequent increase in modulus of elasticity, in the range of 190 to 200 GPa. In addition, AGS have an average resistance limit 200 MPa higher than ADI, which results in a material with a high strength / weight ratio. The microstructures of ADI and AGS consist of ferrite and austenite with high carbon content (ausferrite), instead of ferrite and iron carbide, present in conventional steels. The relative proportion of its microconstituents, and the carbon content present in austenite influences the mechanical properties, especially the wear resistance, since this high-carbon austenite can transform to martensite by deformation. The full potential of using these steels is closely related to the realization of suitable heat treatments, which makes the availability of specific TTT diagrams (time, temperature and transformation) necessary. The influence of alloying elements such as niobium, constitutes another factor to be evaluated. Based on the similarity of behaviors presented by Nb and Mo, the contents of 0.5% and 1.0% of niobium were specified for the present work. In unalloyed steels the bainitic reaction is kinetically "shielded" by the ferritic and pearlite reactions which start at higher temperatures and shorter times, so that in continuous cooling it becomes practically impossible to obtain bainitic structures. Even when isothermal transformation is used it is difficult to obtain bainitic structures, since the ferritic reaction is fast. The addition of some alloying elements usually results in the retardation of the ferritic and pearlitic reactions, often leading to a greater separation of the regions and the reactions in the TTT diagrams, which show their C curves more clearly separated for the ferritic and pearlite reactions. An effective element in this process is Mo, and for a minimum content of 0.5%, there is a marked displacement of the curves referring to the pearlite transformation to the right and the displacement to the left of the bainitic curves. In this work the TTT diagrams of graphitic cast steels with variable niobium contents (without Nb, 0.5%Nb and 1%Nb) were obtained. It was verified that the Nb produced an effect similar to the Mo in this type of steel, displacing the pearlite transformation curves to the right while the bainitic curves were displaced to the left, facilitating the heat treatments of the alloy.

**Keywords:** TTT diagrams, graphitic steel, niobium

# Microstructural study of ODS alloy with hafnium and yttrium addition

Yina Huang, Yucheng Wu, Xiaoyong Zhu, Zhongwei Jin
(Hefei University of Technology)
yina@hfut.edu.cn

**Abstract:** Oxide dispersion strengthened (ODS) steels have been studied intensively for applications in both advanced fission power plants and fusion reactors. This is because of their excellent operation temperature range, improved creep resistance and resistance to radiation damage and gas accumulation. The coherency of dispersoids with the matrix is likely to be important in dislocation-dispersion interactions underpinning strengthening mechanisms.

In this study we have investigated the orientation relationships of dispersoids in a novel ODS alloy, using hafnium rather than, or in addition to, the more conventional yttrium as the basis of the dispersoids. Hafnium has been found to refine the oxide particle size and to improve the homogeneity of the particle distribution. Two alloys, Fe-14Cr-0.22Hf ("14H") and Fe-14Cr-0.25$Y_2O_3$ ("14Y") (compositions in wt%) were investigated, to characterize the micro -structural relationship between dispersoids and matrix.

14H model ODS alloy and 14Y were fabricated by spark plasma sintering (SPS) or hot isostatic pressing (HIP). Electron backscatter diffraction (EBSD) was used to characterize grain sizes and microstructure. Crystal structures and interfacial structures of dispersoids were studied by transmission electron microscopy (TEM), determining orientation relationships between the oxide and the matrix. Micro-chemical profiles of dispersoids and interfaces were examined by scanning transmission electron microscopy–energy dispersive detector (STEM-EDS).

EBSD results show both alloys made by SPS method present uniform grains size shown in Fig.1. Both coarse and fine grains and small grains present in consolidated alloys. Beside these large grains, when comparing numbers of small grains with a diameter around 200 nm-2μm in 14Y exhibits larger and more even grain size than 14H.

Initial TEM analysis shows that dispersoids are homogeneously distributed in the matrix in 14H and 14Y (Fig.2 a and b). Dispersoids in 14H are faceted, with some surface planes of the planes of dispersoids parallel to {110} matrix planes as the diffraction pattern indicated in FFT of Fig.3. STEM ADF analysis shows the average size of dispersoids in 14H is about 2.1nm and density is $0.9\times10^{23}$ /m3, as for 14Y, the average size is about 9 nm and density is $5.8\times10^{21}$ /$m^3$.

From the results, we could conclude that the addition of Hf into a Fe-Cr powder promotes a nanometric distribution of dispersoids. The Hf powder is dissolved in matrix through mechanical alloying and formed Hf-O dispersoids during consolidation. Comparing 14H with 14Y, dispersoids in 14H exhibit higher density with smaller average size. Therefore hafnium shows an alternative addition of element as ODS alloy.

**Keywords:** ODS alloy, processing, microstructure

Fig.1 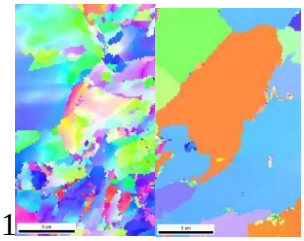 Fig.2 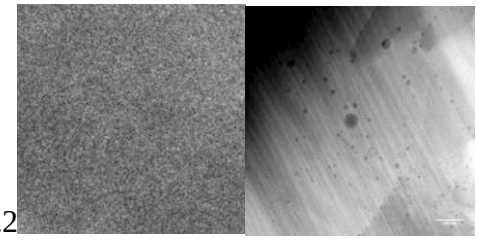 Fig.3 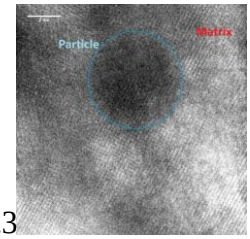


Fig.1 EBSD map of 14H. and 14Y (a. 14H; b. 14YH)
Fig.2 HAADF images of 14H and 14Y
Fig.3 HRTEM of dispersoids and FFT in 14H

# Selection of heat treatment process parameters of H13 hot die steel based on orthogonal test

Wenchao Wang, Yanmin Zhang
(Henan University of Science and Technology)
zhangmin70@163.com

**Abstract:** The hardness, tensile strength and impact toughness of H13 hot die steel were studied by orthogonal design with different quenching temperature (A), first tempering temperature (B) and the second tempering temperature (C) in the heat treatment process. The matrix analysis method was used to calculate the weight of each factor that affects the test results, so as to obtain the optimal heat treatment process. Microstructure and fracture morphology of the alloy treated by optimal process was observed. In order to attain the homogeneous and fine grain of H13 steel spheroidal carbides and excellent comprehensive mechanical properties, isothermal spheroidizing annealing process was adopted: 870 ℃×2 h+750℃×4 h, furnace cooled to about 500 ℃ and then air cooled. H13 steel contains a lot of strong carbide forming elements. The alloying elements is not conducive when the austenitizing temperature of H13 steel is lower than 1000 ℃ or higher than 1070 ℃, therefore, 1020 ℃, 1040 ℃ and 1060 ℃ was selected. The time for heat preservation under the three temperature was all 20 minutes. The three temperatures were used as three levels of factor A in the orthogonal design. Subsequently, two times of high temperature tempering for 2 hour were conducted with temperatures of 580, 600 and 620 ℃, respectively. The three tempering temperatures are selected as the three levels of factor B and C. Thus, a 33 orthogonal table was designed. The hardness, tensile strength and impact toughness of specimens under different quenching and tempering were tested. The microstructure and impact fracture morphology were observed and analyzed by OM and SEM. The test results show that (i) Using the matrix analysis method to analyze the test results of hardness, tensile strength and impact toughness of alloy that selected, it can be seen that: A2 accounts for the largest weight among three levels of factor A; B1 has the largest weight among three levels of factor B; C3 occupies the largest weight among the three levels of factor C. We know that the greater weight, the more obvious of factor impact on the results. Therefore, the best collocation scheme of all the selected heat treatment process parameters is A2B1C3. So, the optimal quenching and tempering process is: 1040 ℃×20 min+580 ℃×2 h+580 ℃×2 h. Under this process, the mechanical properties of H13 alloy were tested: the hardness is 41 HRC, the tensile strength is 990 MPa and impact energy is 68 J. (ii) Microstructural analysis show that under high temperature tempering conditions: the carbide grains gradually grow up, the particle sizes are uneven, the distribution is inhomogeneity, and the dislocations in the lath microstructure are rearranged, resulting in low hardness and good toughness. From the SEM morphology of the impact fracture, it can be seen that there are a large number of tearing ridges, a small amount of shallow and small dimples, and the morphology with quasi-cleavage fracture mechanism.

**Keywords:** H13 hot work die steel, orthogonal test, matrix analysis method, hardness and impact toughness, fracture morphology

# Characterization and optical properties of SnS nano-plate prepared by solvothermal method

Haopeng Jiang
(Harbin Institute of Technology)
707341141@qq.com

**Abstract:** The preparation of photocatalytic materials with high quantum yield and fast response to visible light is currently a research hot-spot in this field. As a kind of narrow band-gap semiconductor material, SnS has light response characteristics in the visible wavelength range, indicating its potential application prospect in the field of photocatalysis. Therefore,we hope to prepare stannous sulfide with photocatalytic effect by simple solvothermal method. The physic-al properties of the materials were investigated using X-ray diffraction (XRD), scanning electron microscopy (SEM), energy dispersive spectroscopy (EDS) and UV-vis spectrometer (UV-vis).

The structure and properties of the materials prepared at different reaction temperatures and reaction times were investigated and showed. The results of XRD syndicate that the product phase compositions change from SnS to β-$SnS_2$ with the increase of reaction ratio of sulfur source. SnS is a Pnma space group in the orthonormal system, and the lattice parameter is in accordance with the theoretical results.

The morphology of SnS powder was shown, nano-plate with thickness of 10-50 nm.

The UV-vis absorption spectroscopy of the SnS nano-plate was shown.

The calculated band gap was about 1.33 eV, which has a certain quantum size effect.

The ability of photocatalytic degradation to RhB solution was tested under the light of 400W metal halide lamp within 3 hours. The results was shown, the peak at 554 nm disappear with the progress of photocatalysis and the degradation rate reached at around 55%.

1) Pure phase SnS powders could be prepared by stannous chloride dehydrate and thiourea under solvothermal conditions, using N, N-Dimethyl formamide (DMF) as solvent. The best condition is at 180 ℃ reaction for 10 hours. The SnS nano-plate prepared shows a good two-dimensional growth trend. The minimum thickness is 10nm.

2) The adsorption capacity of RhB solution on nano-plate SnS was poor, there was a certain ability to catalyze the degradation of RhB. However, it was difficult to further degrade its degradation products.

**Keywords:** SnS, solvothermal

# Effects of niobium addition and aging treatment on the microstructural changes and mechanical properties of the Fe-30Mn-7Al-1.1C alloy

Chungchun Wu, Chuhao Hsu
(Department of Mechanical Engineering, Southern Taiwan University of Science and Technology)
wcc@stust.edu.tw

**Abstract:** The purpose of the present study is an attempt to examine the effects of the 0.5wt% niobium additions on the microstructure and mechanical property of the Fe-30Mn-7Al1.1C Alloy by means of optical microscope (OM), transmission electron microscope equipped with energy-dispersive spectrometry (TEM/EDS), hardness tester and wear resistance tester. The aging processes were performed at the temperatures ranging from 450 ℃ to 750 ℃ for various times. Based on our experimental examinations, it was concluded below. In the asquenched condition, the microstructure of the Fe-30Mn-7Al-1.1C alloy was the single austenite phase. After being aged at 500 ℃ or 550 ℃ for various times, the surface hardness of the Fe-30Mn-7Al-1.1C alloy gradually increased to the maximum valve and then slowly decreased. This result seemed to be related to the precipitation of particle-like (Fe, Mn) 3AlC*x* carbides (defined as κ carbides) on the austenite grain boundary and followed by the phase decomposition of γ to (κ+α) transition with increasing the aging time period. However, the 0.5wt% niobium addition in the Fe-30Mn-7Al-1.1C alloy promoted the mechanical property at high temperature. After being aged at 500 ℃ or 550 ℃ for various times, the surface hardness of the Fe-30Mn-7Al-1.1C-0.5Nb alloy gradually increased to the maximum valve of HRC 43 and then remained the excellent hardness property even for 240 hours or over. Based on our TEM observations, κ carbides preferred to precipitate homogeneously within the austenite matrix instead of form on the austenite grain boundary at 500 ℃ or 550 ℃. After prolong aging processes, κ carbides grew well to appropriate size within the austenite matrix. The phase decomposition of γ to (κ+α) transition decreased significantly. Summary, the niobium addition to the Fe-30Mn-7Al-1.1C alloy not only promoted the homogeneously precipitation of κ carbides within the austenite region but also inhibited the phase decomposition of γ to (κ+α) transition. This result also indicated that the Fe-30Mn-7Al-1.1C-0.5Nb alloy possessed the better service lifetime at 500 ℃ or 550 ℃, which may be substituted as SKD 61 tool steels for some industrial applications.

**Keywords:** Fe-Mn-Al-C alloy, κ carbides, phase decomposition, homogeneously precipitation, niobium addition

# Microstructure and mechanical properties of W-Si composites by spark plasma sintering

Wei Liu, Lihong Xue, Youwei Yan
(Huazhong University of Science and Technology)
xuelh@hust.edu.cn

**Abstract:** Recently, considering an important safety concern in case of a loss-of-coolant accident (LOCA) with simultaneous air ingress into the reactor vessel, self-passivating tungsten alloys, which can form a protection film at the outer surface to prevent the further oxidation of W under this accident, have attracted widely attention. Because of low neutron activation, much low evaporation than $WO_3$, low oxygen permeability among oxides and self-healing properties, W-Si alloys has been recognized as one of the hopeful self-passivating tungsten alloys. The purpose of this work is to make detailed discussion on the microstructure evolution and phase transition progress in W-Si bulk samples. The mechanical properties and deuterium (D) retention behavior of W-Si was also investigated.

Elemental powders of W (99.9% purity, 1-5 μm), Si (99.9% purity, 1-5 μm) were used as raw materials. Nominal compositions of W-*x* at%Si (*x*=3, 5) were mechanical alloying (MA) for 4 h in high-energy planetary ball mill with the rotation speed 250 rpm in argon atmosphere at room temperature (RT). Tungsten carbide balls with ball-to-material weight ratio (BPR) 15:1 and the gradation 1:3 (10 mm and 6 mm diameter, respectively) in sealed cylindrical stainless steel vial were adopted. In addition, 5wt% of ethanol was utilized as process control agent (PCA) to avoid cold welding during MA. After that, milled powders were drying in vacuum oven at 60 ℃for 10 h.

The consolidation of the powders was conducted in spark plasma sintering equipment. Asmilled W-Si powders were sintered at 1650 ℃ for 5 min under 50 MPa in vacuum atmosphere with pulsed DC power (40 ms on and 7 ms off). The size of the sintered samples was 30 mm in diameters and 3 mm in thickness. It was found residual oxygen in powders could be effectively absorbed by Si to form $SiO_2$ particles, resulting in the density increasing. With Si content increasing, tungsten trisilicides were synthesized in-situ and homogeneously distributed in W matrix. According to the Gibb's free energy of related reactions and TGA testing results, it is revealed that Si is easily tending to react with oxygen compared with W. The testing of oxidation resistance shows the formation of tungsten trisilicides can effectively avoid further erosion in W matrix. Moreover, the composites exhibit improved vickers hardness with the addition of Si. Based on indentation results, reinforced phase in W matrix can effectively induce the deflection of crack, which is benefit for the improvement of fracture toughness. Also, it has been found moderate amounts of Si added in tungsten was benefit to reduce the D retention amount.

**Keywords:** W-Si, in situ synthesis, toughness, TDS

# Effect of thermal exposure on microstructure and mechanical properties of an Al-Zn-Mg-Cu alloy

Yanqing Yang[1], Pan Dai[1], Jigang Ru[2]
(1. School of Materials Science & Engineering, Northwestern Polytechnical University;
2. Beijing Institute of Aeronautical Materials)
yqyang@nwpu.edu.cn

**Abstract:** The thermal stability of aluminum alloys for aerospace application is very important due to the harsh working environment such as heavy load, high temperature and high humidity. Therefore, The effect of thermal exposure at the temperature ranging from 100℃ to 175℃ for 500 hours on microstructure and mechanical properties of forged 7A85 alloy thick plate after two-step aging treatment (T7452) are investigated. Based on transmission electron microscopy (TEM) observation and image analysis, it is found that as the exposure temperature increases, the transformation from metastable η′ to equilibrium η occurs and the average precipitate size and the average spacing of neighbor precipitates become larger. The tensile strength, yield strength and hardness increase first and then decrease with the increase of exposure temperature while both the elongation and reduction of area increase.
**Keywords:** Al-Zn-Mg-Cu alloy, thermal exposure, mechanical property, microstructure

# Study on static recrystallization of austenite during hot deformation of heavy rail steel

Lin Chen[1], Mengjie Lou[1], Yuyan Liu[1], Xi Yang[1], Wenqing Yang[2]
(1. Inner Mongolia University of Science and Technology; 2. Baotou North Railway Products Co., Ltd.)
863938085@qq.com

**Abstract:** The softening rate curves of U75V and rare earth heavy rail steels were measured by double pass compression test. The results show that the softening rate curves of U75V and rare earth heavy rail steels increase with the increase of deformation temperature and interval time. When the holding time reaches a certain degree, the softening rate curve will appear platform. In the softening rate curve, the beginning and ending time of the platform correspond to the beginning and ending time of strain induced precipitation.
**Keywords:** Softening rate, recrystallization, back insertion, microalloyed elements

# Formation of high strength and high plasticity nano/ultrafine structure by martensite reversion in 18Cr-8Ni austenitic stainless steel

Jia Liu, Xiangtao Deng, Zhaodong Wang
(State Key Laboratory of Rolling and Automation, Northeastern University)
dengxiangtao123@163.com

**Abstract:** An NG/UFG austenitic stainless steel of type 18Cr-8Ni austenitic stainless steel was produced by strain-induced martensite phase reversion process. Severe cold deformation (70% reduction) at room temperature is carried out, followed by annealing in the conditions of 710 ℃-10 min, 760 ℃-5 min and 950 ℃-5 min. The nano/ultrafine grain size obtained is 400 nm, with the yield strength of 878 MPa and high ductility of 33%. The study of the deformation behavior of CG and NG/UFG steels found that the microstructure at the fracture of NG/UFG steel a great amount of strain-induced martensite and a small number of twins were observed. Whereas, at the fracture of CG steel strain-induced martensite and banded structures with high density dislocations were observed.

**Keywords:** austenitic stainless steel, strain-induced martensite, nano/ultrafine-grained structure

# Aging analysis on low carbon cold rolled steel sheet during rapid heating treatment

Wen Li
(Technology Center of Meishan Iron & Steel Co.)
liwen630376@baosteel.com

**Abstract:** The effect of rapid heating treatment on the aging in three kinds of low carbon cold rolled steel sheets was investigated by using a DIL805A/D thermal dilatometer, including ferrite grain size, austenite transformation temperature point $Ac_1$, $Ar_1$ and carbide precipitation and dissolution. The results indicated that the $Ac_{1s}$ of three samples were all greatly promoted up to 900 ℃, carbon content and initial microstructure had obvious effect on final microstructure and properties when using rapid heating treatment. In addition, through the microstructural analysis of the ferrite grain size and carbide precipitation and dissolution in three samples, it was concluded that aging difference of three samples after rapid heating treatment was greatly relative to their total austenitization and initial carbide properties.

**Keywords:** low carbon cold rolled steel sheet, rapid heating treatment, austenitizing time, aging

# Research on corrosion of 0.3C-14Cr-0.5Ni powder/2Cr13 laser heterogeneous coating

Qiang Li[1], TieMing Guo[1], RuiHua Zhang[2], XiuJie Xu[1], YaBo Pu[1]
(1. Lanzhou University of Technology;
2. Yangjiang Hardware and Cutters Industry and Technology Research Institute)
liqiang930816@126.com

**Abstract:** This paper analyzes the corrosion of the tool in the actual production process. The test standard chooses the brine soak corrosion test of GB/T 15067.2-2016. The discussion of the corrosion phenomena in heat-affected zone (HAZ) and cladding layer was carried out. It was found that the remnants of the tissue segregation and thermal stress had a significant effect on the corrosion of the tool; secondly, the structural defects and structural defects in the cladding layer also affected the corrosion performance of the cladding layer.

**Keywords:** chromium, martensitic stainless steel, dendrite, dendrite

# Effect of solution temperature on microstructure and mechanical properties of Ti-5Al-5Mo-5V-3Cr-1Zr titanium alloy

Chaowen Huang[1], Mingpan Wan[1], Shewei Xin[2], Yongqing Zhao[2]
(1. College of Materials and Metallurgy, Guizhou University;
2. Northwest Institute for Nonferrous Metal Research)
huangchaowen318@163.com

**Abstract:** The purpose of this study is to reveal the relationship of the solution temperature, microstructure and mechanical properties of the Ti-5Al-5Mo-5V-3Cr-1Zr (Ti-55531) titanium alloy. The alloys were prepared by solution at temperature ranging from $T_\beta$-100 ℃ ($T_\beta$, β transus temperature) to $T_\beta$+100 ℃ respectively and aging at 600 ℃ for 6 h. The results indicate that the whole ranging of solution temperature ($T_\beta$-100 ℃ to $T_\beta$+100 ℃) could be divided into following five regions according to its change of strength and ductility of Ti55531 alloy. In region (1) $T_\beta$-100 ℃ to $T_\beta$-50 ℃, with increasing of temperature, the fraction of relatively softer primary α ($\alpha_p$) phase obviously declines, in contrast, the amount of hard β transformed microstructure (β-trans) increases, which leads to the strength of the alloy increases; In region (2) $T_\beta$-50 ℃ to $T_\beta$-30 ℃, the alloy shows the highest strength and good ductility owing to amounts of hard β-trans and certain soft $\alpha_p$; In region (3) $T_\beta$-30 ℃ to $T_\beta$, with increasing of temperature, the strength of the alloy gradually drops due to the quickly increasing length of secondary α ($\alpha_s$) lamellae in β-trans; In region (4) $T_\beta$ to $T_\beta$+60 ℃, with increasing of temperature, the strength of the alloy further drops to a lower level due to the further increasing length of αs lamellae and prior β grain size. Meanwhile, the alloy still presents good ductility; In region (5) $T_\beta$ +60 ℃ to $T_\beta$+100 ℃, it was interested that, with increasing of temperature, the strength of the alloy suddenly dramatically increases to the highest level, while the ductility greatly declines to the lowest level. Therefore, the alloy presenting the excellent mechanical performance combination high strength and good ductility has solution temperatures ranging from $T_\beta$–50 ℃ to $T_\beta$–30 ℃ and from $T_\beta$+10 ℃ to $T_\beta$+30 ℃.

**Keywords:** Ti-55531 titanium alloy, heat treatment, microstructure, mechanical properties

# Comparison of microalloying effects with Ca and Ce on corrosion properties of extruded Mg-3Al-1Zn alloy

Cheng Zhang, Liang Wu, Guangsheng Huang, Xingxing Ding, Bin Jiang, Guangang Wang, Fusheng Pan
(Chongqing University)
wuliang@cqu.edu.cn, gshuang@cqu.edu.cn

**Abstract:** This paper focuses on the microalloying effects of Ca and Ce and comparison of the effects on the corrosion properties of extruded AZ31 alloy. The microstructure and the corrosion behavior are investigated by optical microscope (OM), scanning electron microscope (SEM), hydrogen evolution reaction and electrochemical measurements. Composition analyses are conducted with X-ray fluorescence (XRF), X-ray photoelectron spectroscopy (XPS) and energy-dispersive X-ray spectroscopy (EDS). The microstructure of the AZ31 alloy is greatly modified with the different additions of Ca and Ce (0.2wt%Ca, 0.2wt%Ce, 0.2wt%Ca+0.2wt%Ce), such as grains and second phases. Moreover, protective films with Ca and Ce enrichment are produced on the surface of AZ31 alloys with the microalloying additions of Ca and Ce, which might be a significant factor to affect the corrosion behaviors. The results reveal that the corrosion resistance of extruded AZ31 alloy is improved effectively with the microalloying additions of Ca and Ce. Furthermore, it is remarkable that AZ31-0.2Ca possesses better corrosion resistance than that of AZ31-0.2Ce. Interestingly, compared to AZ31-0.2Ca, the synergistic addition of Ca and Ce cannot improve corrosion resistance further, which is related to different microstructure and composition of corrosion product films.

**Keywords:** microalloying, corrosion, extruded AZ31 alloy, Ca, Ce

# Nanoindentation investigation on the 18Cr-8Ni austenitic stainless steels with grain size from nano/ultrafine-grain to coarse grain

Jia Liu, Xiangtao Deng, Zhaodong Wang
(State Key Laboratory of Rolling and Automation)
1014257803@qq.com, dengxiangtao123@163.com

**Abstract:** Nano-indentation has been a popular technique for measuring the mechanical properties of materials, which can develop the experimental techniques of meso-mechanics. In the present study, the effect of grain size on mechanical properties of 18Cr-8Ni austenitic stainless steel was investigated by nanoindentation technique. The grain size from nano/ultrafine-grain to coarse-grain was obtained by phase reversion process. The uniaxial tensile test and hardness test showed that grain refinement significantly increased the yield strength and Vickers hardness of austenitic stainless steel. From the load-depth (P-h) curves obtained by nanoindentation, mechanical properties such as the indentation hardness ($H$), Young's modulus ($E$), yield strength ($\sigma_{ys}$), strain hardening exponent ($n$) can be analyzed. The result revealed that the grain refinement remarkably influences the elastic–plastic response of the stainless steel to the indentation process. As the grain size decreased, the mesoscopic mechanical properties include $H$, $E$, $\sigma_{ys}$, and $n$ showed increase.

**Keywords:** austenitic stainless steel, nano/ultrafine-grained structure, nano-indentation

# Effect of heat treatment on mechanical property and microstructure of a low nickel superalloy for exhaust engine valves

Yan Mo[1], Wei Wu[1], Dongzhe Wang[1], Haiding Liu[1], Yongyou Li[1], Hong Wan[1], Yinglong Liu[1], Jinhui Song[2], Jintai Wang[2]
(1. Chongqing Materials Research Institute Co. Ltd.;
2. National Engineering Research Center for Instrument Functional Materials)
moyan6868@126.com

**Abstract:** Heavy-duty engines require high performance valve steel. Compared to conventional nickel alloys, such as Nimonic 80A and Inconel 751, low-nickel heat-resistant superalloy is more cost effective. A low nickel superalloy features superb mechanical properties, which are compatible with nickel alloys. However, the performance is strongly related to heat treatment. Therefore, it is necessary to know the details. This study presents the evolution of microstructure and mechanical properties of this superalloy according to heat treatment. We measured the tensile strength, yield strength, elongation percentage, reduction of area, grain size and microstructures of samples performed at different solution and aging heat treatments. From the results, we can see that it is necessary to balance strength and toughness and select appropriate heat treating rules according to detailed application environments of this valve alloy.
**Keywords:** microstructure, property, heat treatment, valve alloy, low nickel, superalloy

# The effect of VC precipitation on the properties of medium carbon high alloyed steel

Xiaoli Zhao, Jianfeng Gu
(Institute of Materials Modification and Modeling, School of Materials Science and Engineering, Shanghai Jiao Tong University)
gujf@sjtu.edu.cn

**Abstract:** The material investigated in this work is AISI H13 steel, this a kind of Cr-Mo-Si-V steel widely used as tools and dies in aluminum injection molding, hot forging, extrusion, and casting process due to its excellent properties such as fracture resistance and strength, high-temperature hardenability, and temper resistance. There are many carbides precipitated during the heat treatment process, because of the high percent of alloyed elements such as Cr, Mo, V in the matrix. And many investigators have paid attention on the effect of carbides on the properties of this steel. As reported, carbides played an important role in improving the impact toughness and strength of steel. In this study, the effect of VC on the properties of AISI H13 steel was investigated.
**Keywords:** carbides, medium carbon high alloyed steel, tensile strength

# Effect of volume fraction of retained austenite on the scratch and abrasion resistance of AISI 321 metastable austenitic stainless steel

Hengyi Zhang, Qiuhong Zhang, Peipei Sun, Chenchong Wang, Wei Xu
(State Key Laboratory of Rolling and Automation, Northeastern University, Shenyang 110819, China)
xuwei@ral.neu.edu.cn

**Abstract:** A systematic experimental investigation was conducted to study the effect of austenite volume fraction on the scratch and abrasion resistance of AISI 321 austenitic stainless steel (ASS). Various volume fractions of retained austenite were introduced by cold rolling at difference reductions. Wear tests were carried out using ball on disc technique at constant velocity but different sliding distances and load conditions. The scratch resistance and corresponding failure mechanisms were evaluated using a micro-scratch test on the in-service work hardening surface which were deformed by the ball on disc abrasion at different load conditions. Correlation between microstructure and wear mechanisms was performed using SEM and X-ray diffraction. Hardness and tensile test were also performed to evaluate the relationship between mechanical properties and wear/scratch resistance. Results show that the scratch resistance does not only depend on the volume fractions of retained austenite, but also the loading conditions employed. The martensite– austenite dual phase steel with an optimized austenite volume fraction yields an even better combination of scratch/abrasion resistance and work hardening ability.

**Keywords:** micro-scratch wear, ball on disc wear, metastable austenitic stainless steels

# Study on aluminum alloy micro-arc oxidation coating thickening reaction mechanism

Wei Song, Bailing Jiang
(Xi'an University of Technology)
jiangbail@vip.163.com

**Abstract:** For obtained excellent anti-wear and anti-corrosion 6061 aluminum alloy coating, anodizing method was used to increase the 6061 aluminum alloy coating thickness, then micro-arc oxidation method was used to compact it. When the 50 mm×50 mm×2 mm 6061 aluminum alloy test block was put into 10% $H_2SO_4$ solutions(*v*/*v*), based on the conditions of electric current density was 4 A/dm$^2$, maintained the solution temperature at 15 ℃ for 80 min, the coating thickness could reach 100 μm. Then the block was put into 3%$Na_2SiO_3$ solution, using NaOH and KOH to adjust the pH value to 12, on the conditions of electric current density was 12 A/dm$^2$, pulse width was 30 μs, the number of the pulse was 1000. When maintaining the solution temperature at 15 ℃ for 15 min, it obtained thick and compact coating, which had been analyzed by XRD. The results proved that it consisted mainly of α-$Al_2O_3$, and the microstructure of the coating had been observed by SEM, which proved that it had dense structure, and the thickness could reach 90 μm.

**Keywords:** aluminum alloy, micro-arc oxidation, thickening, anti-corrosion, anti-wear

# Insight into the microstructure of the surface oxidation layer of nitrogen-rich uranium nitride

Xiaofang Wang[1], Zhong Long[2], Rongguang Zeng[2], Yin Hu[1], Kezhao Liu[1]
(1. Science and Technology on Surface Physics and Chemistry Laboratory;
2. Institute of Materials, China Academy of Engineering Physics)
wangxf_spc@163.com

**Abstract:** Uranium nitrides have aroused great attention for their important application in the corrosion protection of metallic uranium, due to formation of a nanoscale surface oxide layer when exposed to air or an oxygen-including atmosphere that slows or protects against further oxidation, but direct observations on the microstructure of oxide layer and the relationship of the crystal structure between the oxide layer and the underlying uranium nitride remain unresolved. In this work, oxide formation on surface of nitrogen-rich uranium nitride was investigated using X-ray photoelectron spectroscopy (XPS), auger electron spectroscopy (AES), aberration-corrected transmission electron microscopy (TEM), and high-angle annular dark-field scanning transmission electron microscopy (HAADF-STEM) coupled with electron energy-loss spectroscopy (EELS). XPS and AES studies indicated that the oxidized layer on UN2-x film is ternary compound uranium oxynitride (UNxOy) in about 10 nm thickness. TEM/HAADF-STEM and EELS studies revealed the UNxOy crystallizes in the FCC $CaF_2$-type structure with the lattice parameter close to the $CaF_2$-type UN2x matrix. The work can provide further information to the oxidation mechanism of uranium nitride.

**Keywords:** uranium nitride, surface oxidation, uranium oxynitride, STEM-EELS

# A New TiC reinforced low alloy abrasion resistant steel

Long Huang, Xiangtao Deng, Zhaodong Wang
(State Key Laboratory of Rolling and Automation, Northeastern University, Shenyang)
huanglong420@163.com

**Abstract:** A low alloy abrasion resistant steel reinforced with nano and micrometer-size Ti(C, N) particles was processed by thermomechanical controlled processing (TMCP). The microstructure evolution and three-body abrasive wear behavior of experiment steels were studied by SEM, TEM, EPMA and wear testing equipment. The observations reveal that nano and micrometer-size Ti(C, N) particles uniformly distributed in the matrix after TMCP. The micrometer-size particles formed during solidification were beneficial in protecting the matrix from abrasion. The nano-size particles precipitated during TMCP refined the grain size. The abrasion resistance of the experiment steel reinforced with Ti(C, N)-particles was more than 1.5 times of Ti(C, N)-free steel.

**Keywords:** thermomechanical controlled processing, wear, micro particles, nanoparticles

# Processing and properties of nanostructured $TiB_2$-NiCrCoAlY composite powders via spray drying and plasma spheroidization

Zou Yongming[1], Zeng Dechang[1], Wu Yaosha[2], Qiu Zhaoguo[1]
(1. South China University of Technology; 2. Zhongshan Torch Polytechnic)
medczeng@scut.edu.cn

**Abstract:** In this paper, nanostructured $TiB_2$-NiCrCoAlY composite powders were fabricated by spray dry and plasma spheroidization. The properties of powders fabricated via spray dry were compared with the powders fabricated via plasma spheroidization. The results showed that both of them had spherical morphologies, while the latter had stable and dense nanostructure, smooth surface with high sphericity. Both spray dry and plasma spheroidization composite powders were sprayed on stainless steel substrate by high velocity air fuel spray (HVAF). The coatings fabricated from plasma spheroidization powders showed good mechanical properties. Which proved that the powders had good fluidity and suitable for thermal spray.

**Keywords:** plasma spheroidization, spray drying, nanostructured, titanium boride

# Different effect of annealing on the microstructure of supersaturated Cu-Cr alloy film and bulk

Xiaoxue Huang, Haoliang Sun, Yechang Cao, Guangxin Wang, Heinz-Rolf Stock
(Henan University of Science & Technology)
sunhlwm@163.com

**Keywords:** Cu-Cr alloy film, Cu-Cr alloy bulk, annealing, microstructure

**Abstract:** Cu-Cr alloy film and Cu-Cr alloy bulk were prepared by sputtering and vacuum melting, respectively, and some Cu-Cr alloy film and bulk were subsequently annealed. The effects of annealing on the microstructure Cu-Cr alloy film and Cu-Cr alloy bulk were investigated. Results show that the bulk material and alloy film exhibit different microstructure evolution behavior after annealing. The surface morphology of annealed samples clearly shows that submicron faceted Cu particles are self-formed on the annealed Cu-Cr thin film' surface, and Cr dendrite precipitates on the Cu-Cr alloy bulk' surface. The XRD patterns of alloy film indicate no Cr diffraction peaks. In contrast to this, XRD patterns show Cu (111) and Cr (200) peaks in alloy bulks. The difference in microstructure evolution behavior of alloy film and bulk after annealing is discussed.

# Characterization and wear behaviors of SUJ 2 steel in different microstructure

Chiu Liu-Ho[1], Wu Chung-Chun[2]
(1.Tatung University; 2. STUST)
lhchiu@ttu.edu.tw

**Abstract:** Characterization and wear behavior of SUJ2 bearing steels with different microstructure at the same hardness has been investigated. The hardness of the SUJ2 specimens were controlled to a hardness value of 60±0.5 HRC by quenching and tempering with/without cryogenic treatment. Carbide dispersed in the tempered martensite was obtained by austenitizing at 840 ℃, oil quenched and tempered. A combination microstructure of martensite and retained austenite was obtained by austenitized at 940 and 980 ℃, oil quenched and tempered at 200 ℃. The fully martensitic microstructure without carbide can be acquired by a sub-zero treatment. Characterization methods used to identify the difference of SUJ2 specimens at 60 HRC were optical microscopy, eddy current response and X-ray diffraction pattern. The eddy current results can be differentiated according to the amount of retained austenite and martensite. The retained austenite amount can be identified by a μ-X360 diffractometer. Specimens were subjected to a block-on-roller type wear testing with a load of 42 N and 92 N at a speed of 200 rpm. The result of 10000 cycles shows that the full martensitic microstructure by the sub-zero treatment has better wear resistance properties than the quenched and tempered martensite structure with retained austenite.
**Keywords:** heat treatment, eddy current, X-ray diffraction

# Effects of process parameters on content of fluorine and zirconium in oxidation film formed on magnesium alloys

Rongfa zhang, Xiaoting Shi, shufang zhang, Guoqiang Li
(Jiangxi Science and Technology Normal University)
zhang63793@163.com

**Abstract:** Magnesium and magnesium alloys have been studied as a new type biomedical materials for their excellent mechanical properties. Zirconium and Fluorine can effectively improve the corrosion resistance and wear resistance of the anodic coatings. Potassium fluorzirconate has the function of self-sealing holes, which can improve the corrosion resistance of anodic coatings. In this study, F-containing and Zr-containing of oxidation films were formed on magnesium alloys by micro-arc oxidation in the electrolyte with $NH_4HF_2$, Na12Phy and $K_2ZrF_6$. The influence of F-containing and Zr-containing of of anodic coatings was studied by a ΣIGMA FE-SEM and the coating composition was analyzed by EDS. Potentiodynamic polarization test was performed in 3.5wt%NaCl solution to evalulate the corrosion resistance of anodic coatings. The results show that the element F and element Zr increase when the $K_2ZrF_6$ concentration increases. The P-containing increases, but F-containing and Zr-containing decrease with the Na12Phy concentration increasing.
**Keywords:** magnesium alloys, anodic coatings, corrosion resistance, potassium fluorzirconate

# Current status of understanding of alloy element effects on α/γ transformations in steel

M Enomoto

（Ibaraki University, Mito, Japan）

**Abstract:** In the development of advanced steel a great deal of effort has been paid for many years to understand alloy element effects on microstructure formation and mechanical properties. In this presentation, early investigations of alloy element effects and the theory of local equilibrium at moving interfaces are introduced briefly at first. Then, kinetic features which support the local equilibrium assumption in low-alloy steel, and phenomena which seem to indicate the deviation from local equilibrium, such as incomplete transformation of ferrite transformation, will be discussed as well as the factors causing deviation.

1. Theory of local equilibrium at moving interfaces in multi-component low alloy steel
2. Features which support local equilibrium assumption in α/γ transformations
3. Phenomena which indicate the deviation from local equilibrium and factors causing deviation

# Research progress on controlled solidification and its applications

Guang Chen[1], Gong Zheng[1], Zhixiang Qi[1], Jinpeng Zhang[1], Pei Li[1],
Jialin Cheng[2], Zhongwu Zhang[3]
(1. MIIT Key Laboratory of Advanced Metallic and Intermetallic Materials Technology, Engineering Research Center of Materials Behavior and Design, Ministry of Education, Nanjing University of Science and Technology
2. School of Materials Engineering, Nanjing Institute of Technology
3. Key Laboratory of Superlight Materials and Surface Technology, Ministry of Education, Harbin Engineering University)
E-mail: gchen@njust.edu.cn

**Abstract:** This paper reviews the study of our group on controlled solidification and its applications in recent 20 years, including melt heat treatment before solidification, semi-solid processing between liquidus and solidus, rapid progressive solidification of nonequilibrium materials, semi-solid progressive solidification, and directional heat treatment in solid phase transformation. Furthermore, a new technique of material preparation is proposed with the combination of directional solidification and directional heat treatment. In addition, an outlook of controlled solidification technology and its applications are provided.

**Keywords:** controlled solidification, melt heat treatment, semi-solid progressive solidification, directional solidification, directional heat treatment

# Aging behavior of 6061Al matrix composite reinforced with high content SiC nanowires

Wenshu Yang, Gaohui Wu
(School of Materials Science and Engineering, Harbin Institute of Technology)
yws001003@163.com

**Abstract**: After addition of reinforcements, the obtained Al matrix composites usually demonstrate higher specific stiffness and strength than the Al matrix alloys. The aging behavior is also very important to heat treatable Al matrix composites, for instance Al-Mg-Si matrix composites. In the past, the aging behavior of Al matrix composites reinforced with micron-size reinforcements has been deeply investigated. It has been widely found that the introduction of interface between reinforcement and Al matrix has significant effect on the aging behavior of Al matrix. Usually, the interface would only accelerate or delay the precipitation process, and would not alter the precipitation sequence. It has been reported that the aging responses of 0.3 μm $Al_2O_3$/6061Al composites are much lower than that of 6061 alloy, but the precipitation of composites were not changed.

Recently, Al composites reinforced with nano-scale reinforcement has been investigated, the aging behavior of Al matrix is more complex than that in traditional Al composites with micron-size reinforcements. However, K. Kondoh et al. found abnormal aging behavior in extruded carbon nanotubes (CNTs) reinforced 6063Al composites (CNTs content was 0.56 and 1.22 vol%). The hardness, yield and tensile strength of CNTs/6063Al composites were decreased with the increased of CNTs' content after T6 treatment, and Kondoh et al. attributed the degradation in mechanical properties to the segregation of Mg at interface and corresponding interfacial reactions. It has been widely agreed that the high content interface of nano-reinforcement would lead to significant segregation of alloying elements, which would affect the aging behavior of Al matrix. However, the effect and corresponding mechanism have not been fully understood yet. Moreover, the amount of nano-reinforcements reported in literatures is usually lower than 5 wt%, the effect of higher amount nano-reinforcement (corresponding to more interface) has not been investigated yet.

In the present work, the aging behavior of 15 vol% SiCnw/6061Al composite prepared by pressure infiltration method has been investigated. The hardness and tensile properties of SiCnw/6061Al composite was significantly increased after peak-aging treatment, and the addition of high content SiC nanowires have slightly accelerated the aging process. However, the hardness of SiCnw/6061Al composite was decreased much faster (19.4%) than that of 6061Al alloy (10.3%) in the over-aging period. Regardless of heat treatment statuses, SiC/Al interface of SiCnw/6061Al composites was well bonded, and no interfacial product (such as $Al_4C_3$) was found. Spherical (about 3 nm in diameter) and needle (about 2 × 10 nm) GP zones were observed in the under-aged SiCnw/6061Al composites. Afterward, only β" ($Mg_5Si_6$) precipitates with dimension of 4 × 4 nm were detected in the peak-aged SiCnw/6061Al composite (aged 5 h). Furthermore, B' ($MgSi_{>1}$) Precipitates with dimension of 2 × 5 nm were found in the over-aged SiCnw/6061Al composite, which is significant different to that of 6061 alloy and traditional 6061Al matrix composites. After addition of high content SiC nanowires, the precipitation sequence of 6061Al has changed from "GP zones → β" ($Mg_5Si_6$) → β' ($Mg_{1.8}Si$) → β ($Mg_2Si$)" to "GP zones → β" ($Mg_5Si_6$) → B' ($MgSi_{>1}$)". Due to the segregation of Mg at the interface between SiC nanowires and Al matrix, which has been revealed by STEM, the amount of Mg in Al matrix is insufficient Mg amount to form high Mg precipitates, leading to the inhibition of β' and β phases and the formation of B' phase. It could be concluded that the precipitate behavior would be significantly affected by the high content nano-reinforcements due to their higher surface energy and larger surface areas, which might be a characters of high content nano-composites.

**Keywords**: Metal matrix composites; SiC nanowire; Aging; phase transitions; Al-Mg-Si alloys